We are IntechOpen, the world's leading publisher of Open Access books Built by scientists, for scientists

4,800
Open access books available

122,000
International authors and editors

135M
Downloads

Our authors are among the

154
Countries delivered to

TOP 1%
most cited scientists

12.2%
Contributors from top 500 universities

CLARIVATE ANALYTICS BOOK CITATION INDEX INDEXED

WEB OF SCIENCE™

Selection of our books indexed in the Book Citation Index in Web of Science™ Core Collection (BKCI)

Interested in publishing with us?
Contact book.department@intechopen.com

Numbers displayed above are based on latest data collected.
For more information visit www.intechopen.com

14

Estimates of Evapotranspiration and Their Implication in the Mekong and Yellow River Basins

Maichun Zhou
College of Water Conservancy and Civil Engineering, South China Agricultural University, Guangzhou 510642, China

1. Introduction

Potential evapotranspiration (PET) is generally considered to be the maximum rate of evaporation from vegetation-covered land surfaces when water is freely available and is primarily determined by meteorological controls (McVicar et al., 2007; Lhomme, 1997; Granger, 1989). It is a key input to hydrological models. Evapotranspiration can be directly measured by lysimeters or eddy correlation method but expensively and practically only in research over a small plot for a short time. The pan evaporation has long records with dense measurement sites. To apply it in hydrological models, however, first, a pan coefficient, K_p, then a crop coefficient, K_c, must be multiplied. Due to the difference on sitting and weather conditions, K_p is often expressed as a function of local environmental variables such as wind speed, humidity, upwind fetch, etc. A global equation of K_p is still lack. The values of K_c from the literature are empirical, most for agricultural crops, and subjectively selected.

When the environment is water-limited, PET is difficult to measure and therefore is usually estimated as an area-average by the model. If the environment is energy-limited, then the measurement of actual evapotranspiration provides a measure of PET (Donohue et al., 2007). Among the many evaporation models available, the Penman equation (Penman, 1948) and derivation of this equation are preferred, with two extensions being widely employed: (a) the Penman-Monteith equation (P-M) (Monteith, 1965); and (b) the Shuttleworth-Wallace model (S-W) (Shuttleworth and Wallace, 1985). The P-M equation was even standardized as FAO-24 (Doorenbos and Pruitt, 1992) and FAO-56 (Allen et al., 1998) for the reference evapotranspiration of a hypothetical crop. In contrast to many empirical PET formulations of uni- or bi-meteorological variables (e.g. air temperature only of Thornthwaite, 1948; air temperature and solar radiation of Priestley and Taylor, 1972), the P-M and S-W extensions of Penman equation use air temperature, solar radiation, humidity, wind speed, vegetation dynamics, and implicitly consider the influence of feedbacks among forcing meteorological variables, vegetation and evaporation, therefore is physically-based. This chapter compares use of the P-M equation (i.e. the FAO-56 standardized form) and the S-W model over the Mekong and Yellow River basins, representing humid and semi-arid regions, respectively, at a monthly time-step for the period from 1981 to 2000.

2. Methods

2.1 Penman-Monteith (P-M) estimate of reference crop evaporation

The P-M equation treats the vegetation canopy as a single uniform cover or "big-leaf". In its FAO-56 standardized form, the evaporation of a hypothetical crop is estimated (Allen et al., 1998), and hereafter referred to as a reference evapotranspiration (RET) as in Equation (1). The hypothetical crop is assumed: closely resembling an extensive surface of green grass of uniform height (0.12 m), actively growing (canopy resistance of 70 s m^{-1}), completely shading the ground (albedo of 0.23) and with adequate water.

$$RET = \frac{0.408\Delta\left(R_n - G\right) + 900\gamma u_2\left(e_s - e_a\right)/\left(273 + T\right)}{\Delta + \gamma\left(1 + 0.34u_2\right)} \tag{1}$$

where RET is in mm day^{-1}, R_n is the net radiation above vegetation while G is the soil heat flux both (MJ m^{-2} day^{-1}), e_s and e_a are the saturation and actual vapour pressures respectively both (kPa), T is the mean air temperature (^oC), u_2 is the wind speed at 2 m height (m s^{-1}), Δ is the curve slope of relationship between saturation vapour pressure and air temperature (kPa $^oC^{-1}$), and γ is the psychrometric constant (kPa $^oC^{-1}$).

Over a large basin, the big leaf assumption is rarely valid. There are often many vegetation types co-existent, and always some parts or periods where or when the vegetation is not "closed". Both the soil surface and the vegetation leaves evaporate or transpire moisture to the atmosphere and their relative importance changes dynamically as the vegetation develops. The ideal approach is that applicable at all times and places and able to reflect the changes of surface conditions. The S-W model meets this criterion.

2.2 Shuttleworth-Wallace (S-W) model

As an extension of the P-M equation, the S-W model considers dual sources, namely transpiration from vegetation and evaporation from underlying soil (Shuttleworth and Wallace, 1985):

$$\lambda ET = C_c ET_c + C_s ET_s \tag{2}$$

where ET is the total evapotranspiration (mm day^{-1}), λ is the latent heat of water vapourization (MJ kg^{-1}), ET_c and ET_s are equivalent to transpiration and evaporation by applying the P-M model to "closed" canopy and bare substrate respectively (MJ m^{-2} day^{-1}), C_c and C_s are weighting coefficients as functions of resistances. The formulation of all terms in Equation (2) is given as:

$$ET_c = \frac{\Delta\left(R_n - G\right) + \left[\left(24 \times 3600\right)\rho c_p\left(e_s - e_a\right) - \Delta r_a^c\left(R_n^s - G\right)\right]\Big/\left(r_a^a + r_a^c\right)}{\Delta + \gamma\left[1 + r_s^c\Big/\left(r_a^a + r_a^c\right)\right]} \tag{3}$$

$$ET_s = \frac{\Delta\left(R_n - G\right) + \left[\left(24 \times 3600\right)\rho c_p\left(e_s - e_a\right) - \Delta r_a^s\left(R_n - R_n^s\right)\right]\Big/\left(r_a^a + r_a^s\right)}{\Delta + \gamma\left[1 + r_s^s\Big/\left(r_a^a + r_a^c\right)\right]} \tag{4}$$

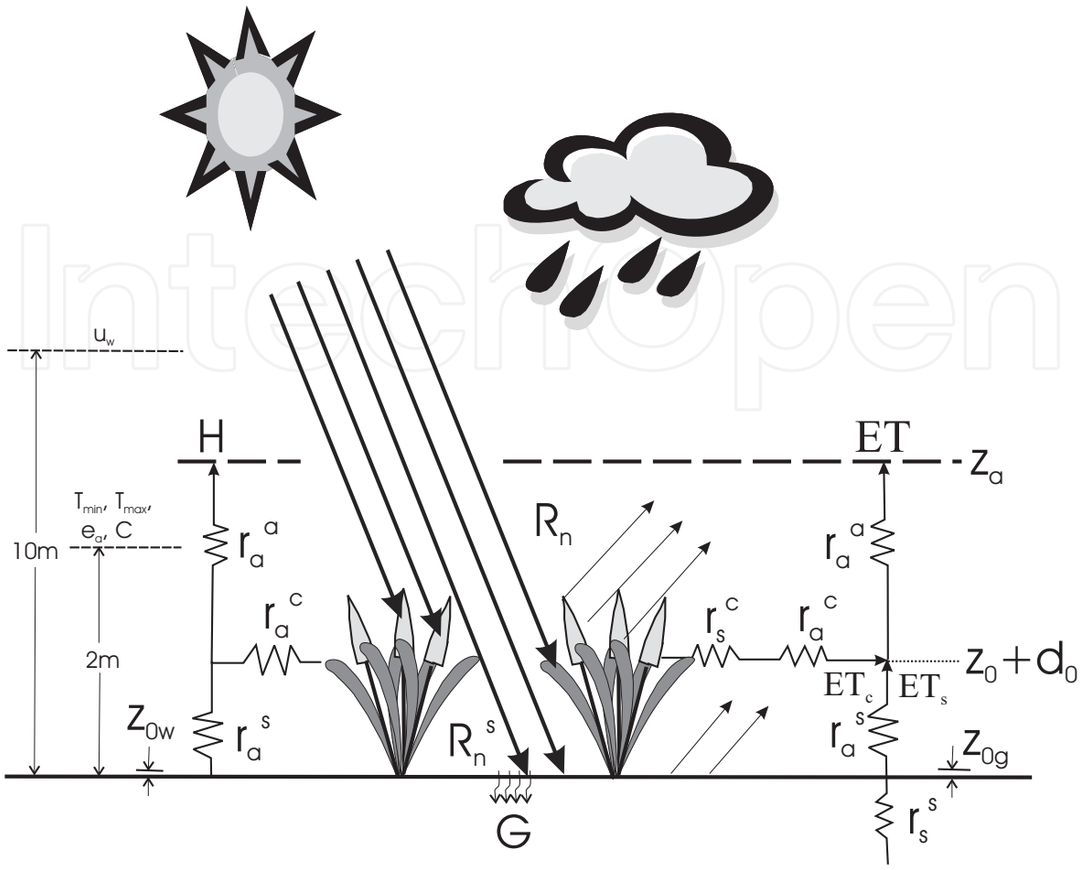

Fig. 1. Schematic diagram of the S-W model. From right to left, r_s^c and r_a^c bulk resistances of canopy stomatal and boundary layer respectively, r_a^s and r_a^a aerodynamic resistances from soil to canopy and from canopy to reference height respectively, r_s^s soil surface resistance, z_{0g} ground roughness length, $z_0 + d_0$ effective height of canopy source, z_a reference height (= h_c + 2 m), h_c vegetation height, R_n and R_n^s net radiations above canopy and to soil surface respectively, G soil heat flux, ET_c transpiration from canopy, ET_s evaporation from soil, ET total evapotranspiration, H sensible heat, T_{min} and T_{max} daily min and max air temperatures respectively, e_a actual vapour pressure, C cloud cover, u_w wind speed at z_w height, h_w observation height for other meteorological variables (usually, z_w = 10 m and h_w = 2 m), z_{0w} ground roughness length at weather station.

$$C_c = \frac{1}{1+\left(R_c R_a\right)/\left[R_s\left(R_c+R_a\right)\right]} \tag{5}$$

$$C_s = \frac{1}{1+\left(R_s R_a\right)/\left[R_c\left(R_s+R_a\right)\right]} \tag{6}$$

$$R_a = \left(\Delta+\gamma\right) r_a^a \tag{7}$$

$$R_c = \left(\Delta+\gamma\right) r_a^c + \gamma r_s^c \tag{8}$$

$$R_s = (\Delta + \gamma) r_a^s + \gamma r_s^s \tag{9}$$

where R_n^s is the net radiation over soil surface (MJm^{-2} day^{-1}), ρ is the mean air density (kg m^{-3}), c_p is the specific heat of moist air (MJkg^{-1} ^{o}C^{-1}), r_s^c and r_a^c are the bulk stomatal and boundary layer resistances of canopy respectively, r_a^s and r_a^a are the aerodynamic resistances between soil and canopy and between canopy and reference height respectively, r_s^s is the surface resistance of soil, all five resistances are in s m^{-1}, other notations are the same as in Equation (1). Figure 1 shows the sensible and latent heat transfer structure of S-W model.

The evaporation from water surface is estimated by substituting the aerodynamic resistance of Penman wind speed function and $r_s = 0$ into the P-M (Shuttleworth, 1993):

$$ET = \frac{\Delta}{\Delta + \gamma} 0.408(R_n - G) + \frac{\gamma}{\Delta + \gamma} 2.624(1 + 0.536u_2)(e_s - e_a) \tag{10}$$

Stannard (1993) and Federer et al. (1996) compared a number of models, including the P-M and the S-W, and found that they give very different prediction. The research of Stannard (1993) and Vorosmarty et al. (1998) shows that hydrological modeling is sensitive to the PET methods, higher in humid regions, and the S-W model performs best. Furthermore, the interception plays an important role in water cycle. Only the S-W model is applicable to the evaporation from interception (Federer et al., 1996). The S-W model, however, is highly complex with many parameters and demands a great deal of data on the meteorology and the land surface characteristics. Most previous work has been focusing on the model validation and comparison with some specific cover types over small experimental catchments in a short time (e.g. Iritz et al., 1999 among others) or in the water balance model at a continent (Vorosmarty et al., 1998). Its application to a large basin for a long term is still lack. In this chapter, first, the S-W model is developed only using parameter values from the literature. Neither experimental measurement nor calibration is introduced. Second, all input data are publicly available, so that it can be applied to the data-poor or ungauged basins, particularly to the large basins. Third, using this method, the spatial distribution of potential evapotranspiration is estimated for a long term over the Mekong and Yellow River basins

2.3 Model parameterization

2.3.1 Climate-related parameters

In Equations from (1) to (10), parameters λ, e_s, Δ, ρ, c_p and γ are directly related to the climatic variables (Shuttleworth, 1993; Allen et al., 1998):

$$\lambda = 2.501 - 0.002361T_s \tag{11}$$

$$e^o(T) = 0.6108 \exp\left(\frac{17.27T}{T + 237.3}\right) \tag{12}$$

$$e_s = \frac{e^o(T_{\max}) + e^o(T_{\min})}{2} \tag{13}$$

$$\Delta = \frac{4098\left[0.6108\exp\left(\frac{17.27T}{T+237.3}\right)\right]}{\left(T+237.3\right)^2} \tag{14}$$

$$\rho = \frac{P}{T_{kv}R} \tag{15}$$

$$P = 101.3\left(\frac{293-0.0065z}{293}\right)^{5.26} \tag{16}$$

$$\gamma = \frac{c_p P}{\varepsilon\lambda} \tag{17}$$

where T_s is the temperature of water surface (°C), substituted with the daily mean air temperature (T) for simplicity, equal to the arithmetic average of $T_{\max}$ and $T_{\min}$, the daily maximum and minimum air temperatures (°C), $e^o(T)$ is the saturation vapour pressure (kPa) at T, Equation (15) is based on the ideal gas law, P is the atmospheric pressure (kPa), assuming 20°C for a standard atmosphere, T_{kv} is the air virtual temperature (K), T_{kv} = 1.01 (273 + T), R is the specific gas constant, 0.287 kJkg^{-1} K^{-1}, z is the elevation above sea level (m), ε is the ratio of the molecular weight of water vapour to that of dry air.
By substituting c_p = 1.013×10^{-3} MJkg^{-1} °C^{-1} (a value under average atmospheric conditions), λ = 2.45 MJkg^{-1} (when the temperature is about 20°C) and ε = 0.622 into Equation (17), the psychrometric constant is approximated as:

$$\gamma = 0.665\times10^{-3}P \tag{18}$$

2.3.2 Aerodynamic resistances

The aerodynamic resistances, r_a^s and r_a^a, are derived by integrating the eddy diffusion coefficients within and above the canopy (K-theory). Shuttleworth and Wallace (1985) applied the K-theory to the complete canopy cover and to the bare substrate soil separately and obtained the final by linearly interpolating between the two limits in terms of LAI, while Shuttleworth and Gurney (1990) applied the K-theory directly to the sparse vegetation canopy through an assumed "preferred" height therefore the interpolation with LAI is unnecessary. Furthermore, Shuttleworth and Wallace (1985) used the "preferred" equations to estimate the roughness length and zero plane displacement of the canopy while Shuttleworth and Gurney (1990) derived them from a second-order closure theory and considered arguably that the latter are superior to the former. In this chapter, the formulation of Shuttleworth and Gurney (1990) is used and the stability effects are ignored to avoid the iterative running of the model, as expressed by Equations (19) and (20). Hess (1998) showed an acceptable estimate for the long-term monthly PET by supposing the sunshine and wind stationary using the P-M method.

$$r_a^s = \frac{h_c\exp(n)}{nK_h}\left[\exp\left(-nz_{0g}/h_c\right)-\exp\left\{-n\left(Z_0+d_p\right)/h_c\right\}\right] \tag{19}$$

$$r_a^a = \frac{1}{\kappa u_*}\ln\left(\frac{z_a - d_0}{h_c - d_0}\right) + \frac{h_c}{nK_h}\left[\exp\left\{n\left[1 - \left(Z_0 + d_p\right)/h_c\right]\right\} - 1\right] \tag{20}$$

where h_c is the vegetation height (m), n is the eddy diffusivity decay constant of the vegetation, K_h is the eddy diffusion coefficient at the top of canopy (m^2 s^{-1}), z_{0g} is the roughness length of ground (m), varying with the vegetation type, Z_0 is the "preferred" roughness length (= $0.13\,h_c$) (m), d_p is the "preferred" zero plane displacement (= $0.63\,h_c$) (m), κ is von Karman's constant (κ = 0.41), u_* is the friction velocity (m s^{-1}), z_a is the reference height (m), 2 m above vegetation, d_0 is the zero plane displacement of canopy (m). All items are parameterized as follows (Monteith, 1973; Choudhury and Monteith, 1988; Shuttleworth and Gurney, 1990; Federer et al., 1996):

$$K_h = \kappa u_* \left(h_c - d_0\right) \tag{21}$$

$$u_* = \kappa u_a \Big/ \ln\left\{\left(z_a - d_0\right)/z_0\right\} \tag{22}$$

$$d_0 = \begin{cases} h_c - z_{0c}/0.3 & LAI \geq 4 \\ 1.1h_c \ln\left[1 + \left(c_d LAI\right)^{1/4}\right] & LAI < 4 \end{cases} \tag{23}$$

$$z_0 = \min\left\{0.3\left(h_c - d_0\right), z_{0g} + 0.3h_c\left(c_d LAI\right)^{0.5}\right\} \tag{24}$$

$$z_{0c} = \begin{cases} 0.13h_c & h_c \leq 1 \\ 0.139h_c - 0.009{h_c}^2 & 1 < h_c < 10 \\ 0.05h_c & h_c \geq 10 \end{cases} \tag{25}$$

$$c_d = \begin{cases} 1.4 \times 10^{-3} & h_c = 0 \\ \left[-1 + \exp\left(0.909 - 3.03 z_{0c}/h_c\right)\right]^4 \Big/ 4 & h_c > 0 \end{cases} \tag{26}$$

$$n = \begin{cases} 2.5 & h_c \leq 1 \\ 2.306 + 0.194h_c & 1 < h_c < 10 \\ 4.25 & h_c \geq 10 \end{cases} \tag{27}$$

where u_a is the wind speed at the reference height (m s^{-1}), z_0 is the roughness length of canopy while z_{0c} is that for a "closed" canopy (m), c_d is the mean drag coefficient for individual leaves. Equations (23) and (24) combine two cases: closed canopy (LAI ≥ 4) and sparse growing vegetation, using the "preferred" values or related to LAI in the second-order closure theory. Equation (25) uses the "preferred" values but differentiates the canopy from short and tall vegetation types and linear interpolated between. Equation (26) uses the value of open water surface for bare surface (Brutsaert, 1982, pp. 118). Wilson and Shaw (1977) assumed c_d as 0.2 for maize leaves, Jones (1992) gave a typical value in the range

between 0.03 and 0.6, whereas Shuttleworth and Gurney (1990) set it to 0.07. Equation (26) gives 0.05 around for short vegetation (h_c < 1 m), but 0.412 for tall vegetation (h_c > 10 m). Equation (27) uses the typical values to represent for short vegetation and tall vegetation, and linear interpolation between: 2.5 of agricultural crop (Monteith, 1973; Uchijima, 1976) and 4.25 of pine forest (Brutsaert, 1982, pp. 106).

The wind speed observed at the weather stations is converted to the reference height using a logarithmic profile in that the internal boundary layer heights over the weather ground and canopy surface are matched and a step change in surface roughness from z_0 to z_{0w} is assumed (Brutsaert, 1982, pp. 59 and pp. 167; Federer et al., 1996):

$$u_a = u_w \frac{\ln(z_b/z_{0w})}{\ln(z_b/z_0)} \frac{\ln\left[(z_a - d_0)/z_0\right]}{\ln(z_w/z_{0w})} \tag{28}$$

where u_w is the wind speed observed at the weather station (m s^{-1}). The height of observation, according to the CRU data (New et al., 1999), z_w is set to 10 m. Over weather station ground, zero plane displacement is assumed zero, the roughness length, z_{0w}, is assumed as 0.005m (Federer et al., 1996), and the height of internal boundary layer, z_b (m), is estimated (Brutsaret, 1982, pp. 165) as:

$$z_b = 0.334 F_w^{0.875} z_{0w}^{0.125} \tag{29}$$

where F_w is the fetch at weather station and assumed F_w = 5000 m.

2.3.3 Bulk stomatal and boundary layer resistances

The bulk stomatal resistance of canopy is affected not only by LAI but also by the environmental variables. It is often expressed as the form (Jarvis, 1976):

$$r_s^c = \frac{r_{ST\min}}{LAI_e \prod_i F_i(X_i)} \tag{30}$$

where LAI_e is the effective LAI, X_i is any environmental variable upon which stomatal response depends, $F_i(X_i)$ is the stress function of X_i , $0 \le F_i(X_i) \le 1$, $r_{ST\min}$ represents the minimal stomatal resistance of individual leaves under optimal conditions (s m^{-1}), for instance, the soil moisture was near field capacity, the temperature was between 17°C and 25°C, the vapor pressure deficit at 2 m level was below 5 hPa and the global radiation was over 400 W m^{-2} (Tourula and Heikinheimo, 1998). In case one or more of stress functions reach zero, r_s^c is given maximum 50000 s m^{-1}, corresponding to the molecular diffusivity of water vapour through leaf cuticula (Tourula and Heikinheimo, 1998).

Shuttleworth and Wallace (1985) expressed the bulk stomatal resistance as $r_s^c = r_{ST}/2LAI$, where r_{ST} is the mean stomatal resistance (of amphistomatous leaves) and LAI is the total leaf area index, and took r_{ST} 400 s m^{-1} for a fully grown agricultural crop (LAI = 4), resulted r_s^c 50 s m^{-1}. Gardiol et al. (2003) used $r_s^c = r_s/2LAI_e$, where $r_s/2$ was considered as the mean stomatal resistance of amphistomatous leaves and LAI_e is equal to $LAI/2$ when $LAI \ge 4$. Gardiol et al. (2003) took r_s 294 s m^{-1} for the corn crop, assuming LAI = 4, resulted r_s^c 73.5 s

m^{-1}. Considering the general crop in Shuttleworth and Wallace (1985) but a specific crop in Gardiol et al. (2003), their equations are actually equivalent. Brisson et al. (1998) used $r_s^c = r_{ST}\sigma_c / LAI$, where σ_c is the shielding factor. If the same value of r_{ST} is used in both Shuttleworth and Wallace (1985) and Brisson et al. (1998), σ_c is equivalent to 1/ 2. However, Brisson et al. (1998) used r_{ST} 250 s m^{-1} for the maize crop and expressed the shielding factor $\sigma_c = 0.5LAI + 1$. Considering the actually adopted large value for r_{ST} and another expression for σ_c, the equation of Brisson et al. (1998) is also equivalent to that of Shuttleworth and Wallace (1985). Unifying these equations, the bulk stomatal resistance can be expressed $r_s^c = r_{ST}/LAI_e$, where the use of LAI_e means only the upper leaves of canopy are active in heat and vapour transfer due to illumination-induced stomatal closure deep in the canopy (Allen et al., 1993). It should be noted that r_{ST} takes implicitly accounts for the environmental effects. If explicitly, Equation (30) is used. LAI_e is calculated equal to actual LAI for $LAI \le 2$, $LAI/2$ for $LAI \ge 4$ and 2 for intermediate LAI (Gardiol et al., 2003).
For the environmental stress functions, CO_2 concentration is ignored and others are outlined as follows:

$$F_1(S) = (dS)/(c+S) \tag{31}$$

$$F_2(D) = \begin{cases} 1 - 0.409D & \textit{for short vegetation} \\ 1 - 0.238D & \textit{for tall vegetation} \end{cases} \tag{32}$$

$$F_3(T) = \begin{cases} 1 & T \ge 298 \\ 1 - 1.6\times 10^{-3}(298 - T)^2 & 273 < T < 298 \\ 0 & T \le 273 \end{cases} \tag{33}$$

$$F_4(\theta) = \begin{cases} 1 & \theta \ge \theta_f \\ \dfrac{\theta - \theta_r}{\theta_f - \theta_r} & \theta_f < \theta < \theta_r \\ 0 & \theta \le \theta_r \end{cases} \tag{34}$$

As shown in Equation (31), the hyperbolic solar radiation function is used (Jarvis, 1976; Stewart, 1988; Stewart and Gay, 1989), where S is the incoming photo-synthetically active radiation (PAR) (in the range of 0.4-0.72 microns) flux (W m^{-2}), $d = 1 + c / 1000$, c = 100 for forests and 400 for crops. For simplicity, the net radiation rather than the solar irradiation is used (Monteith, 1995) and averaged for the day time in daily simulation. The coefficient of vapour pressure deficit function, Equation (32), is represented for short vegetation obtained from the Konza Prairie in Kansas (FIFE data) (Stewart and Gay, 1989), and for tall vegetation by the coniferous forest from the Hydrologic Atmospheric Pilot Experiment/ Modelisation du Bilan Hydrique (HAPEX-MOBILHY) data (Noilhan and Planton, 1989; also see Lhomme et al., 1998), where $D = e_s - e_a$. When the air temperature, T, is higher than 25°C, the stomatal openness is not limited; less than 0°C, stomatal closes completely; and varies linearly between, as shown in Equation (33) where T in K. The stress function of soil moisture content is shown in Equation (34), where θ is the soil moisture content in root

zone, θ_f is the field capacity below which the transpiration is stressed, θ_r is the residual soil moisture content. For PET estimation, the soil moisture is assumed at field capacity.
The bulk boundary layer resistance of canopy is calculated equivalent to all leaf boundary layers in parallel (Shuttleworth and Wallace, 1985; Brisson et al., 1998):

$$r_a^c = r_b \sigma_b / LAI \tag{35}$$

where σ_b is the shielding factor, taking 0.5 (Shuttleworth and Wallace, 1985; Brisson et al., 1998), r_b is the boundary layer resistance of individual leaf and is obtained as (Shuttleworth and Gurney, 1990):

$$r_b = \frac{100}{n}\left(\frac{w}{u_h}\right)^{1/2}\left[1-\exp\left(-n/2\right)\right]^{-1} \tag{36}$$

where r_b is in s m^{-1}, w is the canopy characteristic leaf width (m), u_h is the wind speed at the top of canopy (m s^{-1}), estimated using Equation (28) by substituting h_c for z_a, and n is the eddy diffusivity decay constant (see Equation (27)).

2.3.4 Surface resistance of substrate soil

Monteith (1981) proposed a two-layer model to simulate the soil evaporation, namely a drying soil layer overlaying a wet soil layer. The soil surface resistance is interpreted the resistance for the water vapour to diffuse through the dry top layer from the "evaporative front", the level of wet soil layer. It has been observed that a dry top layer developed quickly after a rainfall event in one day or even in a few hours, but very thin not extending a few centimeters (Hiller, 1980, p. 122; van de Griend and Owe, 1994; Lund and Soegaard, 2003). This is also supported by the finding of Stannard (1993) that the surface resistance was unrelated to the shallow soil moisture (at a depth of 0.15 m). Not only the soil physical parameters (such as moisture, vapour pressure and temperature gradients, matric forces, pore diameter, etc.) but also the air turbulence at the soil atmosphere interface affect this rapid process. It is most difficult, if not impossible, to develop the very detailed models which require a very high vertical resolution on the order of 1 mm close to the soil-atmosphere interface in order to describe the continuity of water fluxes properly. Consequently, to simplify the problems, Choudhury and Monteith (1988) calculated the soil surface resistance using the depth of upper dry soil, Equation (37), while van de Griend and Owe (1994) using the topsoil moisture, Equation (38):

$$r_s^s = \tau l / \left(pD_v\right) \tag{37}$$

$$r_s^s = 10\exp\left[\alpha_\theta\left(\theta_{\min}-\theta\right)\right] \quad \theta \le \theta_{\min} \tag{38}$$

where l is the depth of upper dry layer (m), p is the porosity, τ is the tortuosity factor, D_v is the molecular diffusion coefficient for water vapour (m^2 s^{-1}), θ is the soil moisture content (percent by volume) in the top 1 cm, and $\theta_{\min}$ is an empirical minimum value above which the soil is able to deliver vapour at a potential rate, α_θ is a coefficient. The value of 10 in Equation (38) represents the resistance to molecular diffusion across the water surface itself.

Due to the lack of research on the parameters (τ , p , D_v , $\theta_{\min}$ and α_θ) for different soil types and the difficulty to determine the variables (l and θ), it is not practical at the moment to apply Equations (37) and (38) to large basins. Therefore, r_s^s is set to 500 s m^{-1} for PET estimation, as Shuttleworth and Wallace (1985) and Federer et al. (1996) did. This value is reasoned by that (a) Fuchs and Tanner (1968) suggested between 1000 and 2500 s m^{-1} for a sandy soil with a dry surface layer of 1.5 cm; (b) Camillo and Gurney (1986) found that a resistance between 100 and 600 s m^{-1} significantly improved the performance of a bare soil evaporation model; (c) Kondo et al. (1990) suggested that the surface resistance can exceed 4000 s m^{-1} for a very dry soil layer of 2 cm depth; (d) Mahfouf and Noilhan (1991) reported r_s^s could vary between 0 and several thousands second per meter; (e) when the wilting moisture θ_r = 4.1% (Rawls and Brakensiek, 1985) is used for θ , Equation (38) gives r_s^s 486 s m^{-1} where van de Griend and Owe (1994) used $\theta_{\min} = \theta_{field}/2$ = 15% and α_θ was calibrated as 0.3563 for a fine sandy loam; (f) Lund and Soegaard (2003) found that on the first day after rain the soil resistance increases from 0 in the morning to about 500 s m^{-1} by the end of the day in a millet field with a sandy loam; (g) when θ_r = 4.1 % and θ_{sat} = 45.3 % (Rawls and Brakensiek, 1985) are used, the empirical equation of Sun (1982) gives r_s^s 417 s m^{-1} for the sandy loam.

2.3.5 Net radiations over vegetation canopy, substrate soil surface and soil heat flux

Net radiation over vegetation canopy As a combination method, the reliability of S-W model is largely dependent on the accuracy of net radiation. However, the measurement of net radiation over large areas is impracticable but can be estimated from the solar radiation:

$$R_n = R_{ns} - R_{nl} \tag{39}$$

$$R_{ns} = \left(1-\alpha\right)R_{solar} \tag{40}$$

$$R_{nl} = \sigma\left(\frac{T_{\max,k}^4 + T_{\min,k}^4}{2}\right)\left(0.34 - 0.14\sqrt{e_a}\right)\left(1.35\frac{R_{solar}}{R_{solar}^0} - 0.35\right) \tag{41}$$

where R_{solar} , R_{solar}^0 and R_{ns} are the solar, clear-sky solar and net solar radiations respectively, R_{nl} is the net loss of energy in longwave radiation to the atmosphere, α is the albedo of land surface, σ is the Stefan-Boltzmann constant (= 4.903×10^{-9} MJ K^{-4} m^{-2} day^{-1}), $T_{\max,k}$ and $T_{\min,k}$ are the max and min atmospheric temperatures in Kalvin, $T_{\max,k}$ = $T_{\max}$ + 273.16 and $T_{\min,k}$ = $T_{\min}$ + 273.16. All radiation terms are in MJ m^{-2} day^{-1}. R_{solar} depends on the Julian date, the latitude location and the cloud cover condition (see Appendix A). In Equation (41), the first term is based on the Stefan-Boltzmann law, second term is the net emissivity between the atmosphere and the land surface, and third term is the correctness factor for the cloud cover (Shuttleworth, 1993; Allen et al., 1998). The land surface albedo is related to vegetation LAI (Uchijima, 1976) as:

$$\alpha = \alpha_m - \left(\alpha_m - \alpha_s\right)\exp\left(-0.56LAI\right) \tag{42}$$

where α_m and α_s are the albedo corresponding to the "closed" canopy and the bare soil, respectively. For PET estimation, α_s = 0.1 is used for the wet bare soil (Shuttleworth, 1993) and α_m is from the literature and changes with the vegetation types.

Radiation flux over substrate soil surface The radiation reaching soil surface, R_n^s, can be calculated using a Beer's law relationship of the form

$$R_n^s = R_n \exp\left(-C_r LAI\right) \tag{43}$$

where C_r is the extinction coefficient of the vegetation for net radiation. Monteith (1973) arbitrarily chose 0.7. Denmead (1976) gave 0.5-0.7 for the wheat and was cited by Kelliher et al. (1995). Lafleur and Rouse (1990) reported the value in a range from 0.3 to 0.8 and Ross (1975) from 0.3 to 0.6. Brisson et al. (1998) obtained C_r = 0.25 ± (0.001) for a well watered soybean crop by calibration, which is less than the value generally admitted (0.25 instead of 0.4, Shuttleworth and Wallace, 1985; Braud et al., 1995), due to the soil surface water status. If the soil dries out, its temperature and albedo increase, leads to a decrease in soil net radiation. Both Stannard (1993) and Mo et al. (2004) took 0.5. It is convenient to ignore variation in C_r which occurs in response to structural differences of vegetation, thus, C_r = 0.5 is also used here.

Soil heat flux The heat conduction into the substrate is commonly taken about 30% of R_n^s (Stannard, 1993). However, it is found too much in our monthly simulation. Accordingly, the equation of Allen et al. (1998) is used:

$$G = 0.07\left(T_{i+1} - T_{i-1}\right) \tag{44}$$

where T_{i-1} and T_{i+1} are the mean air temperatures in previous and next months respectively (°C).

2.3.6 Vegetation parameters

Except the soil surface resistance, all other resistances and each component of radiation are related to the vegetation parameters such as LAI, height and leaf width. Vegetation morphology changes dynamically with the environmental conditions (e.g. the prolonged water stress) and seasons. Probably, only the satellite can efficiently provide a frequent measurement to the time-varying vegetation in a long term and over a lager area.

Leaf area index (LAI) The LAI is used not only intensively in S-W parameterization but also in interception estimation. The LAI for each vegetation class can be derived from NOAA-AVHRR NDVI through FPAR (Myneni and Williams, 1994; Sellers et al., 1994; Andersen et al., 2002). Here the SiB2 method is used (Sellers et al., 1996):

$$SR = \frac{1 + NDVI}{1 - NDVI} \tag{45}$$

$$FPAR = FPAR_{\min} + \left(FPAR_{\max} - FPAR_{\min}\right)\frac{\left(SR - SR_{\min}\right)}{\left(SR_{\max} - SR_{\min}\right)} \tag{46}$$

$$LAI = \left(1 - F_{cl}\right)LAI_{\max}\frac{\ln\left(1 - FPAR\right)}{\ln\left(1 - FPAR_{\max}\right)} + F_{cl}LAI_{\max}\frac{FPAR}{FPAR_{\max}} \tag{47}$$

where SR is the simple ratio of hemispheric reflectance for the NIR (near-infrared) light to that for the visible light, $FPAR$ is the fraction of photo-synthetically active radiation, F_{cl} is

the fraction of clumped vegetation, $SR_{\min}$ and $SR_{\max}$ are SR with 5% and 98% of NDVI population. The values of F_{cl}, NDVI at 5% and 98% population are adopted from SiB2 for all vegetation types (NDVI at 5% setting to 0.039 globally, F_{cl} and NDVI at 98%, see Table 1). $FPAR_{\min}$ = 0.001 and $FPAR_{\max}$ = 0.950 consider the satellite-sensed NDVI saturation (Sellers et al., 1996). $LAI_{\max}$ is the maximum LAI when the vegetation develops fully, prescribed for each vegetation class by referring to the literature.

Vegetation height The vegetation height is calculated by differentiating the annual and perennial vegetation. For perennial vegetation, the height is assumed constant; but for the annual, the height grows with the LAI in a linear relationship, although an exponential relationship has also been used by some investigators (e.g. Brisson et al., 1998):

$$h_c = \begin{cases} 0 & LAI_{\max} = 0 \ (\textit{water surface}, \textit{bare soil}, \textit{etc.}) \\ h_{c\min} + \left(h_{c\max} - h_{c\min}\right)\dfrac{LAI}{LAI_{\max}} & LAI_{\max} \neq 0 \end{cases} \tag{48}$$

where $h_{c\min}$ and $h_{c\max}$ are the minimum and maximum vegetation heights prescribed by referring to the literature. For the perennial vegetation such as the forests, shrubs, etc., the same value is prescribed to $h_{c\min}$ and $h_{c\max}$.

Leaf width The leaf width is also treated by differentiating the annual and perennial vegetation. For annual vegetation, it is calculated using an exponential relation with LAI (Farahani and Bausch, 1995):

$$w = \begin{cases} w_{\max} & \textit{for perennial vegetation} \\ w_{\max}\left[1 - \exp\left(-0.6LAI\right)\right] & \textit{for annual vegetation} \end{cases} \tag{49}$$

2.3.7 Prescribed parameters

In S-W model parameterization, we need to prescribe a number of threshold parameters for vegetation canopy and roughness length of substrate soil surface. They are listed in Table 1 for IGBP (Global International Geosphere-Biosphere Programme) land cover classification by referring to the literature and our general knowledge, mainly from

1. α_m: Brutsaert (1982), Shuttleworth (1993), Fennessey and Kirshen (1994)
2. $LAI_{\max}$: Vorosmarty et al. (1998) (3.6 for shortgrass, 4.1 for tall grass, 5.2 for woodland, 5.0 for deciduous forest, 4.4 for evergreen forest and 1.6 for alpine), Andersen et al. (2002) (7 for evergreen broad leaf forest and 5 for other vegetation), Vourlitis et al. (2002) (6 for tropical rain forest and 1 for savanna), and so on
3. h_c, $w_{\max}$, F_{cl} and $NDVI_{98\%}$: Sellers et al. (1996) and Mo et al. (2004)
4. $r_{ST\min}$ (s m^{-1}): McNaughton and Black (1973) (75 for Douglas fir forest), Korner et al. (1979) (90-100 for barley crop), Calder et al. (1986) (120 for rain forest), Verma et al. (1986) (75-160 for deciduous forests), Rowntree (1991) (40-60 for growing crop, 80-130 for forests and 60-200 for grassland), Allen (1994) (100 for grass), Huntingford (1995) (82.6-125 for savanna), Kelliher et al. (1995) (80-90 for crop, 125 for grassland, 160-220 for forests), Vorosmarty et al. (1998) (90 for cultivated lands and 190 for forest and savanna), and Shen et al. (2002) (128 for wheat crop) among many other investigators

5. z_{0g} : Federer et al. (1996)
6. A number of parameters consisting of above items: Noihan and Planton (1989), Liang et al. (1994), Dunn and Mackay (1995), Raupach (1995), Mauser and Schadlich (1998)

Code	Type	α_m	LAI_{max}	h_c (m)	w_{max} (m)	F_{cl}	$r_{ST\text{-}min}$ (s m^{-1})	$NDVI_{98\%}$	z_{0g} (m)
1	Evergreen needleleaf forests	0.16	5.5	17.0-17.0	0.001	1.0	150	0.689	0.020
2	Evergreen broadleaf forests	0.20	7.0	30.0-30.0	0.05	0.0	150	0.611	0.020
3	Deciduous needleleaf forests	0.15	3.3	17.0-17.0	0.001	1.0	150	0.689	0.020
4	Deciduous broadleaf forests	0.18	7.0	25.0-25.0	0.08	0.0	150	0.721	0.020
5	Mixed forests	0.17	5.7	20.0-20.0	0.04	0.5	150	0.721	0.020
6	Closed shrublands	0.20	4.6	1.5- 1.5	0.01	0.0	150	0.674	0.020
7	Open shrublands	0.15	3.0	1.0- 1.0	0.01	1.0	100	0.674	0.020
8	Woods savannas	0.20	1.5	0.8- 0.8	0.01	0.5	180	0.611	0.020
9	Savannas	0.25	0.9	0.1- 0.8	0.01	0.8	120	0.674	0.020
10	Grasslands	0.23	1.8	0.05-0.8	0.01	0.0	115	0.674	0.010
11	Permanent wetlands	0.10	6.0	0.05-1.0	0.01	0.0	65	0.674	0.010
12	Croplands	0.20	7.0	0.0- 0.8	0.01	0.0	90	0.674	0.005
13	Urban and built-up	0.18	----	------	-----	0.0	0	0.674	0.020
14	Cropland/ natural vegetation mosaic	0.20	6.5	0.1- 0.8	0.01	0.5	120	0.674	0.010
15	Permanent snow and ice	0.70	----	------	-----	0.0	0	0.674	0.001
16	Barren or sparsely vegetated	0.15	0.3	0.05-0.8	0.01	1.0	120	0.674	0.001
17	Water bodies	0.08	----	------	-----	0.0	0	0.674	0.001

Code is IGBP number for vegetation type, α_m is maximum albedo (full cover), LAI_{max} is maximum leaf area index, h_c is vegetation height (a function of LAI), w_{max} is maximum vegetation leaf width, F_{cl} is fraction of clumped vegetation, $r_{ST\,min}$ is minimum stomatal resistance of individual leaf, z_{0g} is roughness length of substrate ground. Perennial vegetations: codes from 1 to 8, and annual vegetations: others; tall vegetations: codes from 1 to 5, and short vegetations: others.

Table 1. Land cover threshold parameters, NDVI at 98% population, and ground roughness length of substrate surface based on the IGBP classification from the literature

3. Study region description

The Mekong River, see Figure 2, is the longest river in Southeast Asia and the 12th longest river in the world, with a length of 4 800 km, a drainage area of 805 604 km^2 (WRI et al., 2003), and with an annual runoff of 475×10^9 m^3. It originates on the Tibetan Plateau and flows southwards through China, Myanmar, Laos, Thailand, Cambodia, and Vietnam before it discharges into the South China Sea. The upper Mekong River (1 600 km, from the Tibetan

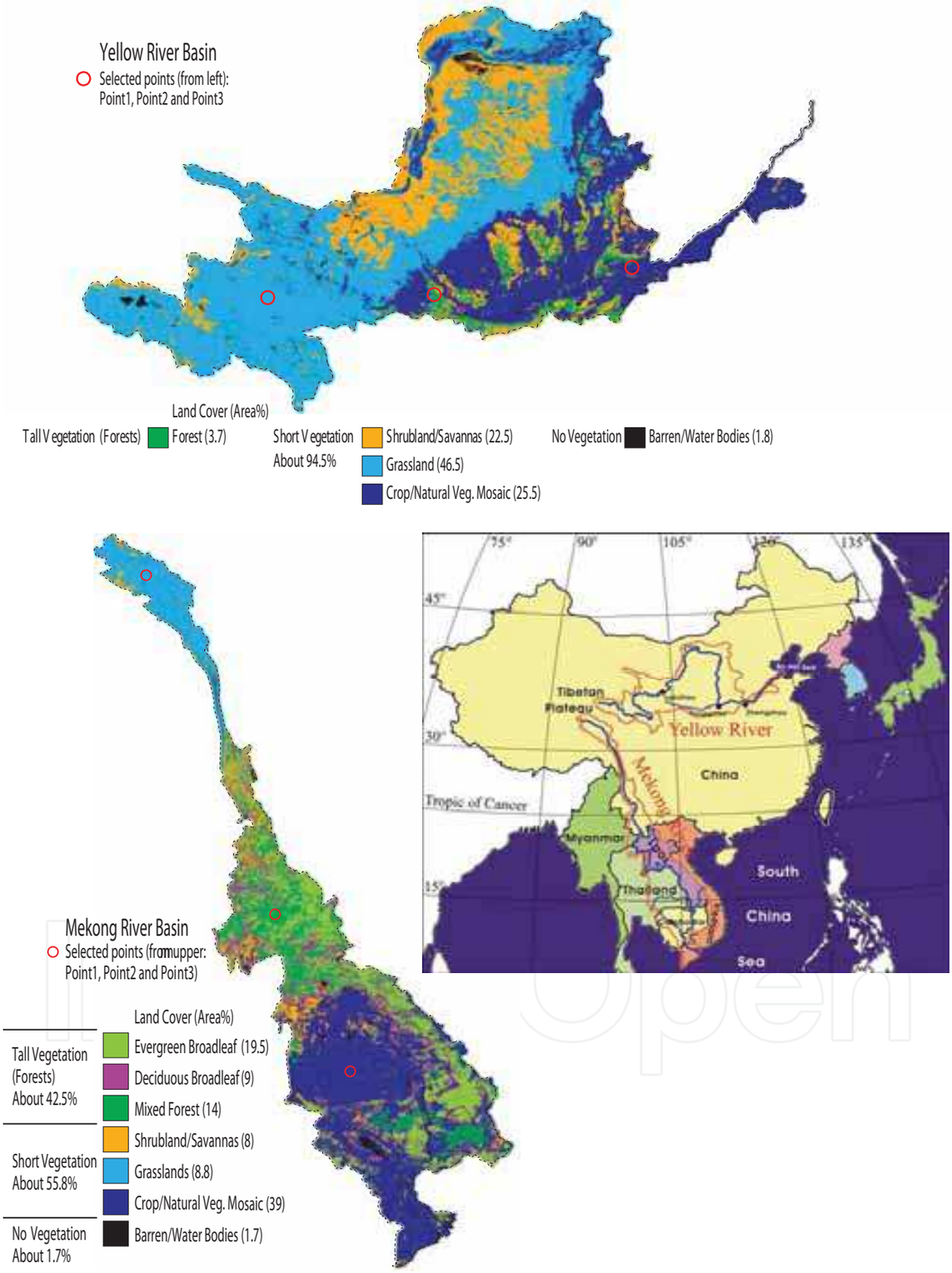

Fig. 2. Mekong and Yellow basins in Asian monsoon region: main streams, IGBP land cover, and selected points.

Plateau to the Thailand-Myanmar border), called the Lancang River in China, drops rapidly by about 4 500 m in a series of large mountain ranges. After exiting China and entering the Golden Triangle (an area of around 350 000 km^2 overlapping mountains of four countries: Myanmar, Laos, Vietnam, and Thailand), it is called the Lower Mekong River. The Lower Mekong River is gentle and most of its reaches are navigable. The climate of upper Mekong River basin has a high-mountainous cold weather with mean annual precipitation from about 300 mm at its source on the Tibetan Plateau to 1600 mm before entering the Golden Triangle. The lower Mekong River is situated in the tropics and is dominated by two distinct monsoons: the southwest from Indian Ocean from mid-May to mid-October with frequent rainfall, and the northeast from China from mid-October to April with a dry spell. The mean annual rainfall in the lower Mekong River ranges from 1 000 mm in northeast Thailand to more than 3 200 mm in the mountainous regions in Laos (Kite, 2001), and around 85-90% of it falls during the rainy season.

The Yellow River, see Figure 1, is the second longest river in China, with a length of 5 464 km, draining an area of 794 712 km^2, and with an annual runoff of 58×10^9 m^3. The Yellow River is divided into upper (2 119 km, from the source to Lanzhou), middle (2 571 km, from Lanzhou to Zhengzhou) and lower (774 km, from Zhengzhou to the Bo Hai Sea). The upper river winds around a series of large mountain ranges on the eastern Tibetan Plateau falling more than 3 300 m and basin average elevation about 4 000 m. After Lanzhou, the river makes a large northern loop through the alluvial plains and the Loess Plateau to Tongguan, picking up more than 90% of its silt load (3 kg m^{-3} at Lanzhou increasing to 35 kg m^{-3} at Tongguan). The lower river is narrow and flows within levees and dikes which have been constructed over the past 2000 years. Sediment deposition from the highly erosive Loess Plateau has continuously increased the height of the river bed. In places, the river bottom is 20 m above the surrounding land surface. The Yellow River basin has an arid and semi-arid continental monsoon climate. In the upper basin, the temperature is a complicated function of the elevation and low throughout the year. In the middle basin, the temperature decreases from south to north and from east to west, and is affected by local mountains and deserts. In the lower basin, the climate is dry and windy in spring, hot and wet in summer, dry in fall, and moderately cold and dry in winter. The annual precipitation is between 200-650 mm over the basin, being large in the lower basin and in the southern portion of the upper and middle basins.

4. Data sources

In order to apply the P-M equation and S-W model, topographic data, characteristics of land cover and meteorological data are required.

4.1 Topographic data

The P-M equation and S-W model use a DEM (Digital Elevation Model) to calculate the parameters of atmospheric pressure, mean air density and psychrometric constant. The Hydro1K DEM was downloaded (http:/ / lpdaac.usgs.gov/ gtopo30/ hydro/ index.html) and clipped to the basins defined by manual digitization from the DCW (Digital Chart of the World) (http:/ / www.maproom.psu.edu/ dcw; Danko, 1992). It is a hydrologically correct DEM developed at the Data Center of USGS EROS (Earth Resources Observation System, U.S. Geological Survey) (Verdin and Greenlee, 1996). Original topography at 1-km resolution was averaged on to an 8-km grid, i.e. the same resolution as NDVI (Normalized Difference Vegetation Index, see following).

4.2 Land cover

The IGBP (International Geosphere-Biosphere Programme) land cover dataset is used to characterize the basin land surface (http:/ / edcwww.cr.usgs.gov/ landdaac/ glcc/ glcc.html) (see Figure 2). It was derived from 1-km AVHRR data (Advanced Very High Resolution Radiometer) spanning April 1992 through March 1993 by the Data Center of USGS EROS, the University of Nebraska-Lincoln and the Joint Research Centre of the European Commission (Loveland et al., 2000). The IGBP categories the global land covers into 17 classes. To show the prevailing types, some minor land covers are classified into the similar types in Figure 2. In the Mekong River basin, the most common land cover is forests (~42.5%), the second most common is croplands or a mosaic of cropland and natural vegetation (~39%). Most of remainder is shrubland or grassland (each ~8%). In the Yellow River basin, the most common land cover is grassland (~47%), the second most common is croplands or a mosaic of cropland and natural vegetation (~26%), while the forested area is very small (< 4%). Most of remainder is shrubland or savanna (~23%). The original 1-km spatial resolution was converted to an 8-km grid by assigning the most common land cover to each 8-km cell. While the aggregation from 1-km to 8-km changes the proportion of land cover types to some extent, the general spatial distribution remains.

4.3 NDVI data

Monthly NOAA-AVHRR maximum NDVI composite data at 8-km grid resolution (ftp:/ / daac.gsfc.nasa.gov/ data/ avhrr/ global_8km/ ; Tucker et al., 2005) was obtained from July 13, 1981 to September 21, 2001, except for a period with missing data from September to December 1994. The NDVI data for the basins were transferred into Lambert Azimuthal Equal Area projection. The monthly NDVI data are assumed to represent the value for the middle day of the month. The average monthly NDVI data from 1981 to 2000 are used during the period when data were missing.

4.4 Meteorological data

The required meteorological data include air temperature, relative humidity, radiation and wind speed. The CRU (Climate Research Unit, University of East Anglia in UK) TS 2.0 dataset provides monthly time series of mean air temperature, diurnal air temperature range, precipitation, cloud cover, and actual vapour pressure from 1901 to 2000, and mean wind speed from 1961 to 1990 globally on a 0.5-degree grid (New et al., 1999 and 2000). The wind speed was mainly measured at 10 m height (New et al., 1999). CRU TS 2.0 dataset was interpolated as a function of latitude, longitude, and elevation (TBASE 5-min latitude–longitude global DEM at http:/ / www.ngdc.noaa.gov/ seg/ topo/ topo.shtml) from station data using thin-plate splines (Hutchinson, 1995) for the 1961-1990 climatic normals and angular distance–weighted for the monthly anomalies relative to the 1961–1990 mean in which the influence of elevation was ignored. The climatic variables were separated into two categories: primary and secondary (New et al., 1999). The primary data variables include mean air temperature, the diurnal air temperature range and precipitation, which were constructed directly from station observations. The secondary variables used include cloud cover and vapour pressure, which were constructed by merging station observations (where available) with synthetic data derived from the gridded primary variables. In the synthetic data, cloud cover was related to the diurnal air temperature range, and the actual vapour pressure to the daily minimum air temperature (New et al., 2000). The CRU data sets were

extracted for the basins and transferred into Lambert Azimuthal Equal Area projection at 8-km resolution without interpolation.

All the climatic variables change significantly throughout the year and are very non-uniformly distributed across the basins. Figure 3 shows the general characteristics of six monthly climatic variables: maximum and minimum air temperatures (T_{max} and T_{min} in ^{o}C), precipitation (P in mm/ month), actual vapour pressure (e_a in kPa), cloud cover (C in tenth), and wind speed (u in m s^{-1}). They were spatially and temporally averaged over the whole basins and from 1981 to 2000 (T_{max}, T_{min}, P, e_a and C) or from 1961 to 1990 (u). The Mekong River basin spans from 33.5^{o}N to 9.0^{o}N, crossing from the cold mountainous climate in the Tibetan Plateau to the hot tropical climate in the Indochina Peninsula. Although the Yellow River basin also originates from the Tibetan Plateau, it generally flows at constant latitude. In the Mekong River basin, a large proportion is located in the tropics, whereas almost the whole Yellow River basin sits in North China. Their climate patterns are very different. In the two basins, the coldest points are both located in the Tibetan Plateau, as shown by the similar monthly change of the lower dash lines in Figures from 3(a) to 3(d). The maximum point temperature occurs at the center of middle Yellow River and at the center of Lower Mekong, respectively. The basin-spatially averaged temperature (solid lines in Figures from 3(a) to 3(d)) and maximum cell temperature (upper dash lines in Figures from 3(a) to 3(d)) change similarly. In another words, basin-spatial average T_{max} and cell T_{max} peak in March and April in the Mekong River basin (Figure 3(a)), and in June and July in the Yellow River basin (Figure 3(b)). In the Mekong River basin, the cell T_{min} (upper dash line in Figure 3 (c)) peaks almost constantly from April to October (basin rainy season) but the basin-spatial average T_{min} peaks from June to August due to the weight of cold region in Tibetan Plateau. In the Yellow River basin, both cell T_{min} and basin-spatial average T_{min} peaks in July, the same as in the case of its T_{max}. Most precipitation occurs from May to October in both basins (Figures 3(e) and 3(f)). Accordingly the vapour pressure and cloud cover are high during this time (Figures from 3(g) to 3(j)). The general pattern of relative humidity is governed by the southeast rainy monsoon from the Indian Ocean from mid-May to mid-October in the Mekong River basin, and by the rainy monsoon from the Indian and Pacific oceans during summer months in the Yellow River basin. Basin-wide mean relative humidity is more constant throughout the year in the Mekong (Figures 3(g)), with much larger variation being seen in the Yellow River basin (Figures 3(h)). The almost zero minimum relative humidity in both basins is located in the Tibetan Plateau. The monthly distribution of wind speed, u, is uni-modal for the minimum, weekly bi-modal for the basin-spatial average and the maximum both in the Mekong and Yellow River basins due to the two distinct monsoons, with a strong peak in April and a weaker peak in November, see Figures 3(k) and 3(l).

To compute the solar radiation, the cloudiness, C (tenth), is converted into the relative sunshine duration using the relationship of Doorenbos and Pruitt (1992), as shown in Table 2 and fitted in Equation (50).

$$\frac{n}{N} = 0.9234 - 0.048C - 0.0042C^2 \tag{50}$$

where n and N are actual and maximum possible sunshine duration (hour day^{-1}).

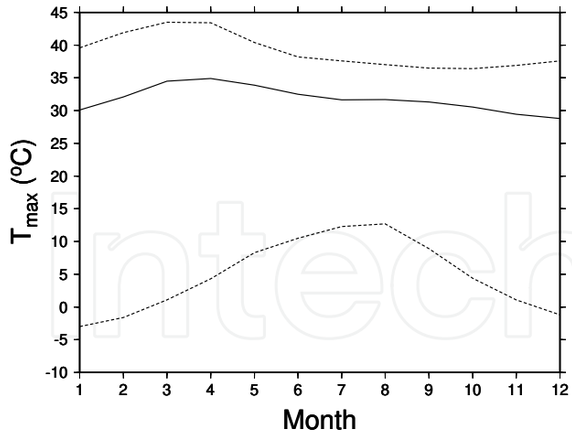

(a) T_{max} over Mekong

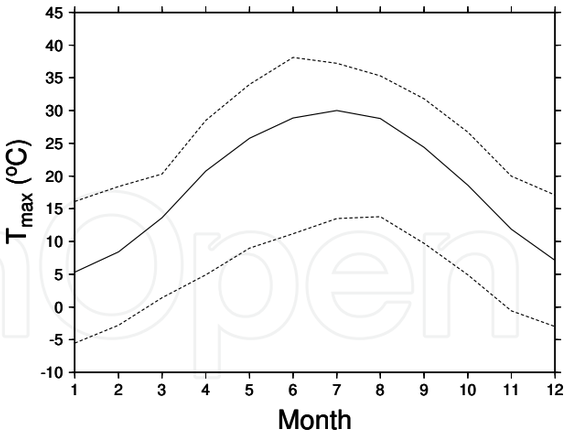

(b) T_{max} over Yellow

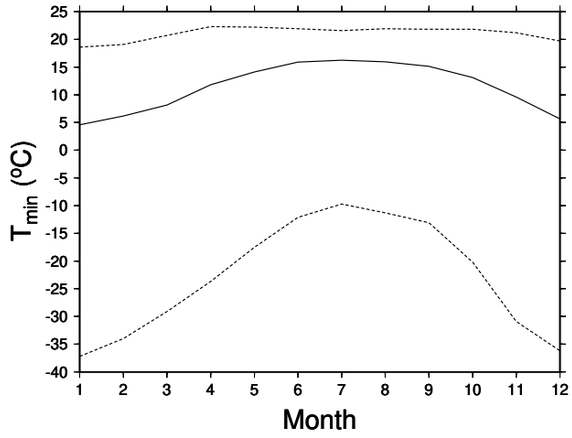

(c) T_{min} over Mekong

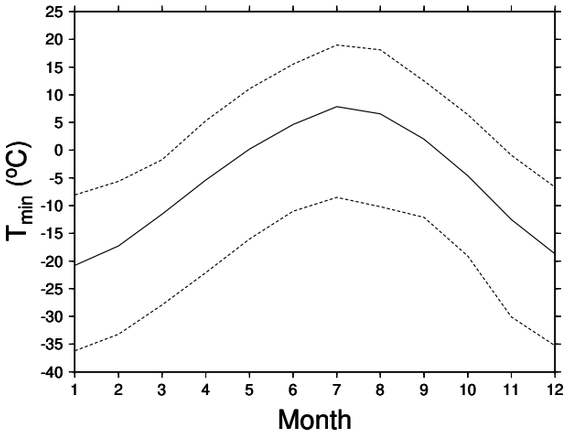

(d) T_{min} over Yellow

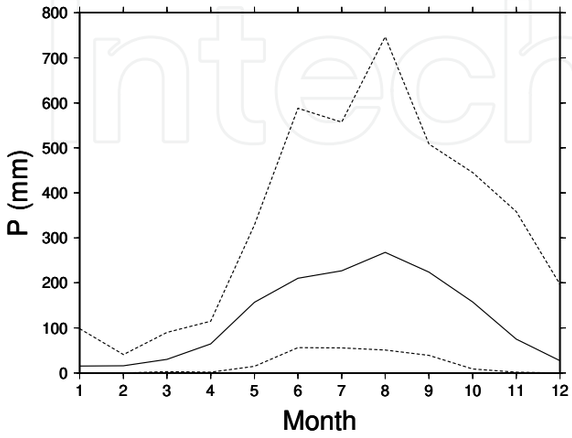

(e) P over Mekong

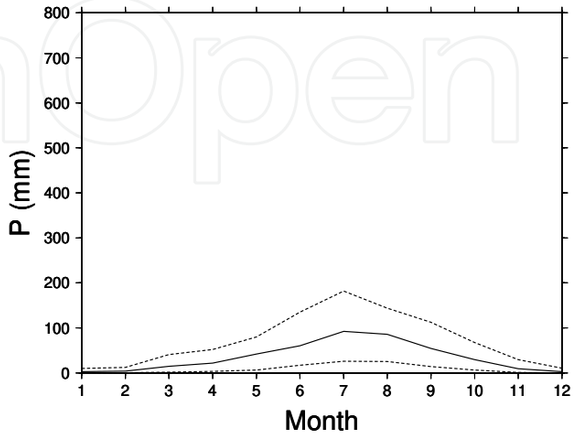

(f) P over Yellow

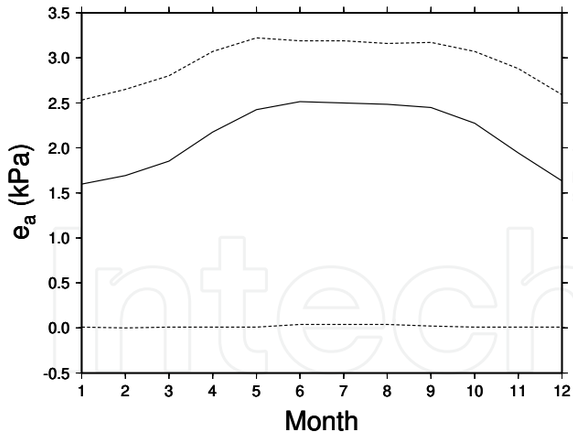

(g) e_a over Mekong

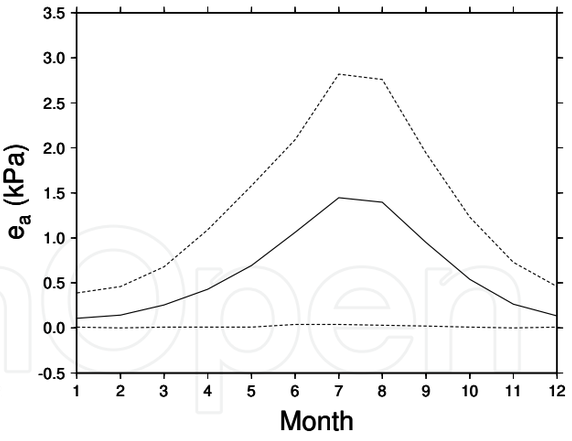

(h) e_a over Yellow

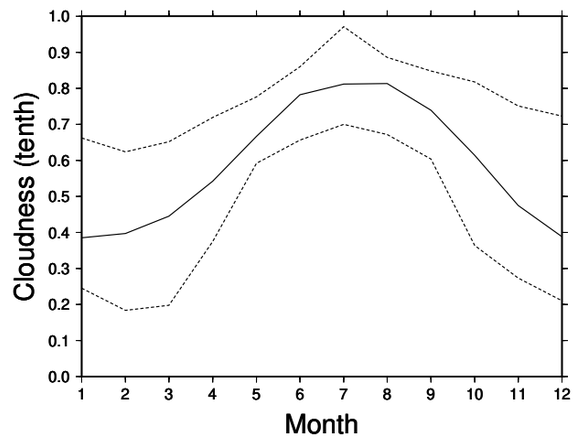

(i) C over Mekong;

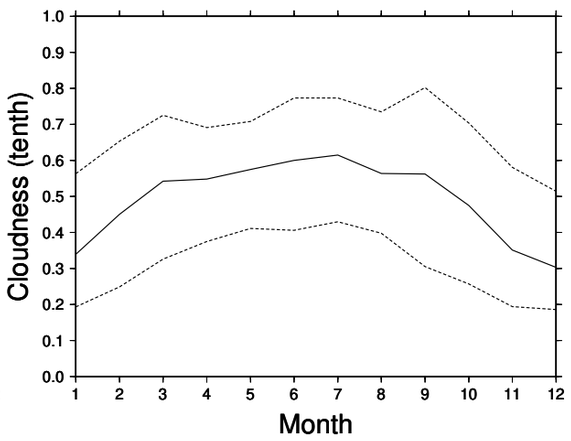

(j) C over Yellow

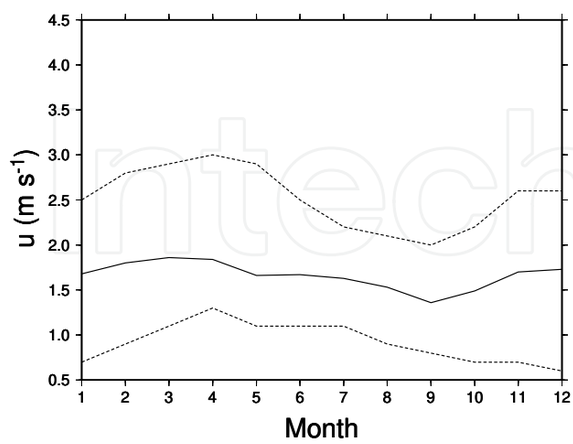

(k) u over Mekong

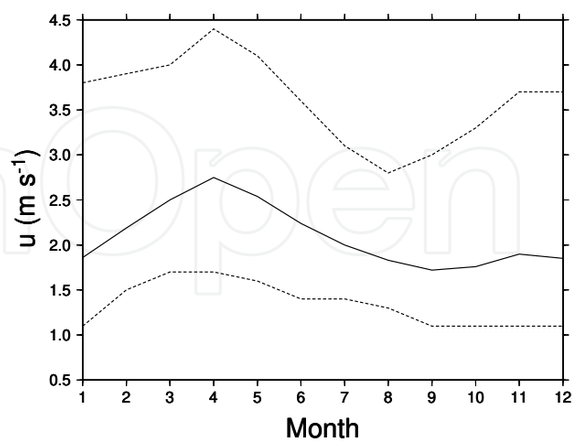

(l) u over Yellow

Fig. 3 Monthly climatological variables: T_{max}, T_{min}, P, e_a and C are averaged during 1981-2000, and u is averaged during 1961-1990; The spatial mean (solid line), the spatial minimum and maximum (dash lines) are shown.

Cloudiness (tenth)	0	1	2	3	4	5	6	7	8	9	10
n/ N	0.95	0.85	0.8	0.75	0.65	0.55	0.5	0.4	0.3	0.15	0

n/ N is the ratio of actual sunshine duration to maximum possible hours of sunshine.

Table 2. Relationship between cloud cover and sunshine duration (source: Doorenbos and Pruitt, 1992)

The 1961-1990 monthly mean wind speed data are used for whole 1981-2000 simulation period, we acknowledge that changes in RET and PET due to recently reported decreases in terrestrial tropical and mid-latitude near-surface wind speeds (McVicar et al. 2008) need to be accounted for when considering longer temporal extents. The wind speed at reference height (2 m height above the ground in FAO-56 equation and 2 m height above the vegetation canopy in S-W model) is converted using Equation (28).

5. Results and discussion

5.1 Comparison of spatial distributions of PET and RET and their interrelationships

The basin-average RET and PET, shown in Figure 4 for the period from 1981 to 2000, both reflect a similar variability and trend in climate. The good linearity between RET and PET, see Figure 5, means that about 70~80% of the inter-annual variability in basin-average PET can be explained by variations in climate, the remaining 20~30% being determined by vegetation diversity and dynamics which are incorporated in the S-W model but not in the FAO-56 P-M method. However, the spatial distributions of RET and PET are strikingly different, see Figure 6. The RET reflects the three climatic patterns over the individual basins: upper, middle and lower. On the other hand, these climatic patterns are not so clearly displayed in the PET distribution, but the effect of vegetation is more obvious. To clearly show the difference between RET and PET, the spatial distributions of average annual (RET-PET) and (RET-PET)/ PET are displayed in Figure 7. Over the Tibetan Plateau of Mekong River basin where the actual vegetation of grassland has a lower LAI than the hypothetical reference crop, RET is estimated higher than PET because a lower LAI means more soil surface uncovered and the resistance of soil surface used in PET is much higher than the resistance of reference crop (500 m s^{-1} vs. 70 m s^{-1}). Over the Lower Mekong River basin where the large forest area has a higher LAI than the hypothetical reference crop, RET is lower than PET because a high LAI means soil surface covered well and the combined resistance of forest and soil surface is small (high LAI reducing the bulk stomatal resistance of forest canopy significantly, see Equation (30)). The vegetation morphology (forest being tall and grass being short) and LAI also affect the land surface albedo, then R_n. The estimate of RET is lower 120 mm/ year (or only 1.7%) than PET basin-spatially (Figures 7(a) and 7(c)). Over the Yellow River basin, because there are few forests (see Figure 2) and the short vegetation generally has a lower LAI (due to water shortage), RET is estimated to be much higher than PET, basin-spatially 300 mm/ year (or about 50%) (Figures 7(b) and 7(d)).

Three specific locations representing typical vegetation types were investigated in greater detail, namely, grass (Point 1), forest (Point 2) and crop (Point 3), see Figure 2. The aggregation of resolution from 1-km to 8-km does not change the vegetation types of these points. The year-to-year changes in both RET and PET are similar at the grass and forest points in the Mekong, and at all three points in the Yellow, that is when RET increases, in most cases PET also increases, and *vice versa*, see Figure 4. But at the crop point over the Mekong, the variation of amplitude in annual PET is not so large as in annual RET during 1985 to 1996, probably

because the grass and forests are natural but the crop is also affected by irrigation, cultivation and human maintenance, with a heavy weight in the Mekong but a light weight in the Yellow comparing with the climate controls. However, the inter-annual changes are larger in PET than in RET at the three points in the Mekong and at the grass and forest points in the Yellow. Reasons are anticipated that: (a) vegetation types amplified or diminished the climatic effects on PET (e.g. the forest vs. the hypothetical crop, or the grass in the Tibetan Plateau vs. the hypothetical crop); (b) vegetation dynamics as a feedback of forcing meteorological controls changed the climatic effects on PET (see the following section).

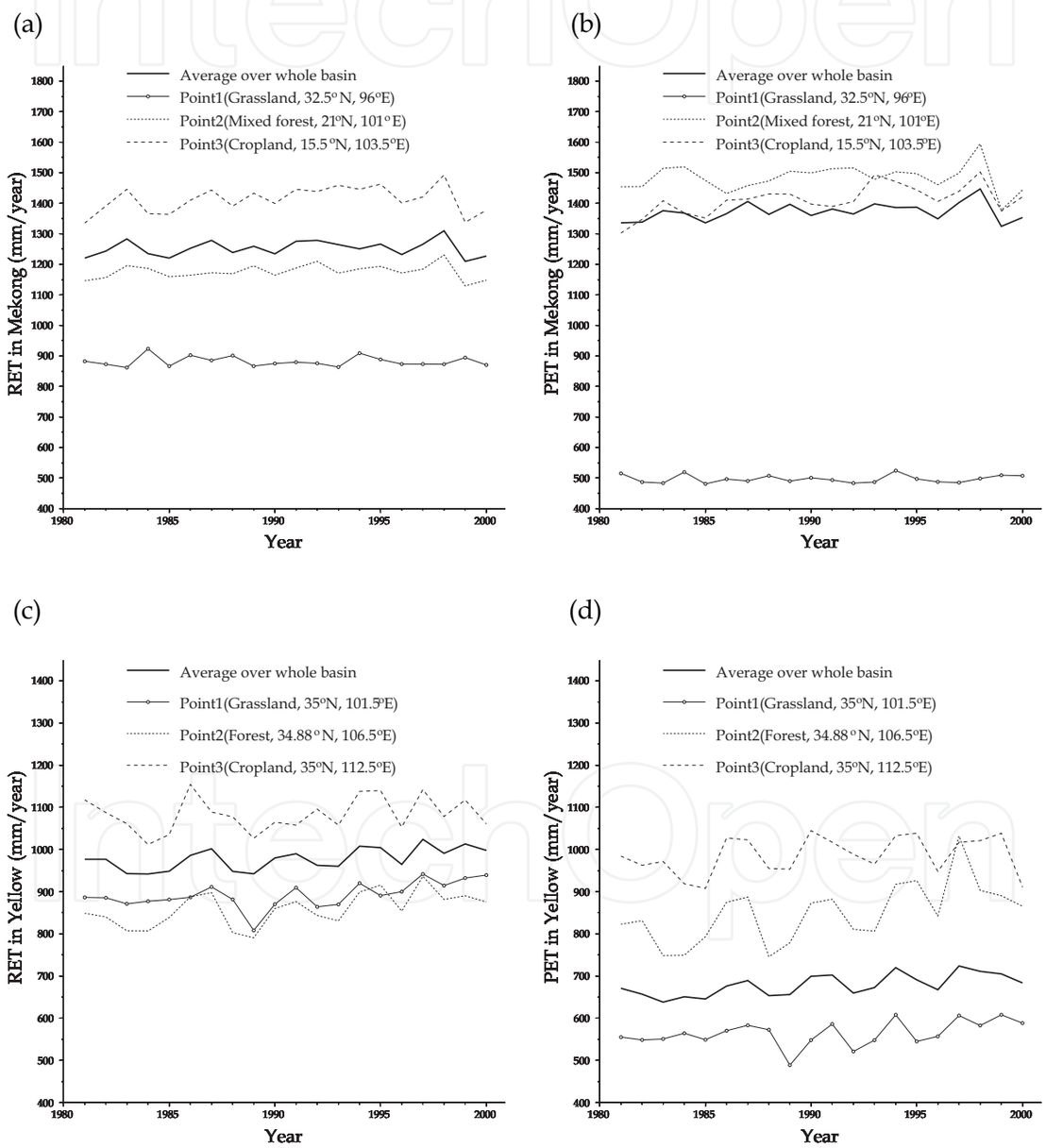

Fig. 4. Year-to-year change of annual RET and PET over whole basins and at three selected points in 1981-2000: (a) RET in Mekong; (b) PET in Mekong; (c) RET in Yellow; (d) PET in Yellow.

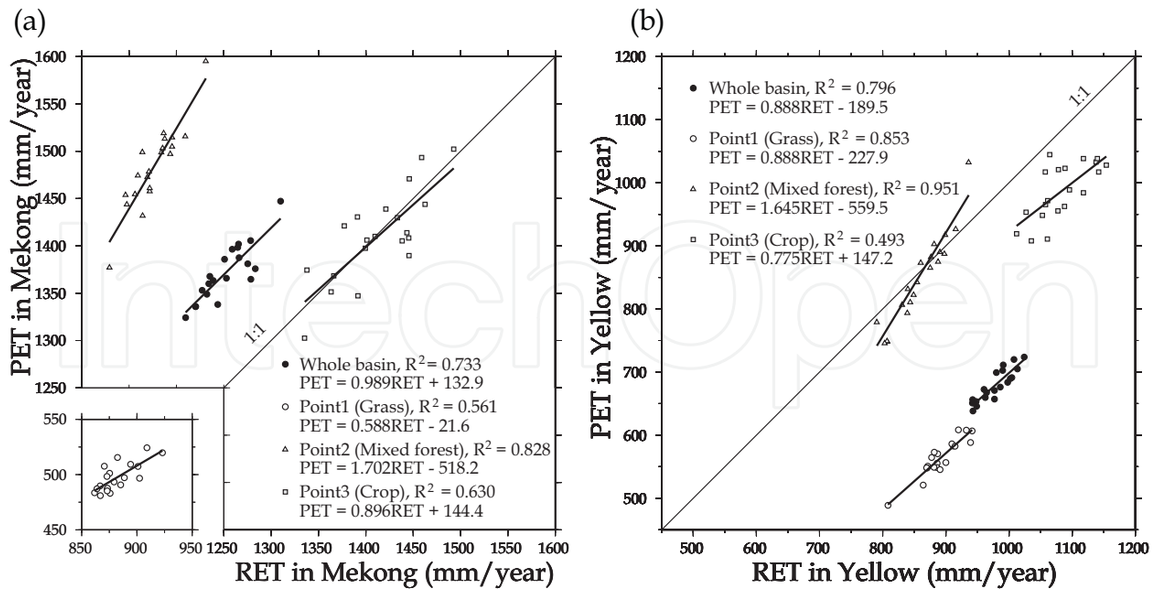

Fig. 5. Relationship between annual RET and PET over whole basins and at three selected points in 1981-2000: (a) RET vs. PET in Mekong; (b) RET vs. PET in Yellow.

5.2 Potential evapotranspiration for vegetation interception

By the S-W model, the potential evapotranspiration from interception, PET_0, is estimated with $r_s^c = r_s^s = 0$. In Mekong River basin, the ratio of PET_0/ PET is 1.63 in average, with 2.90 for grassland, 1.74 for forests and 1.32 for cropland. PET_0 is much higher than the interception storage capacity, I_{max}. For example, PET_0 is about 7.3 mm day^{-1} in average in Mekong River basin but I_{max} is only 1.4 mm from $I_{max} = C_{int}$ LAI when 7.0 is used for LAI_{max} with the forests (see Table 1) where C_{int} is the interception coefficient and $C_{int} = 0.2$ mm is used (Dickinson, 1984; De Ridder and Schayes, 1997; Vazquez and Feyen, 2003; Mo et al., 2004), assuming one rainfall occurs one day. The interception storage controls its actual evaporation. In Yellow River basin, the ratio of PET_0/ PET is 2.65 in average (much larger than in Mekong River basin because of the poor vegetation in favor of PET_0 but not PET relatively), with 2.69 for grassland, 3.40 for forests and 1.98 for cropland.

5.3 Implication of cyclical S-W estimates over Yellow River basin

PET at the forest and crop points in the Yellow River basin changes cyclically (Figure 4(d)), driven by the seasonal precipitation effect on the vegetation development. To show this, the relationship between seasonal vegetation LAI and seasonal precipitation is analyzed over a large area (i.e. the whole Loess Plateau in the middle reaches of Yellow River, gray shaded area in Figure 8) in order to avoid that the point vegetation is easily affected by local and surrounding factors (e.g. runoff from neighbouring grids). The forest point is located inside the Loess Plateau and the crop point close to the Loess Plateau. The vegetation LAI over the Loess Plateau in the middle Yellow River is estimated from NDVI data in Equations from (45) to (47). The regional average precipitation is calculated from the weather station observation (black points in the gray shaded area of Figure 8) using the Thiessen polygon method. As shown in Figure 9(c), the point vegetation LAI in warm and wet seasons (LAI_{wet}) changes similarly to the Loess Plateau vegetation LAI_{wet} but not exactly and with

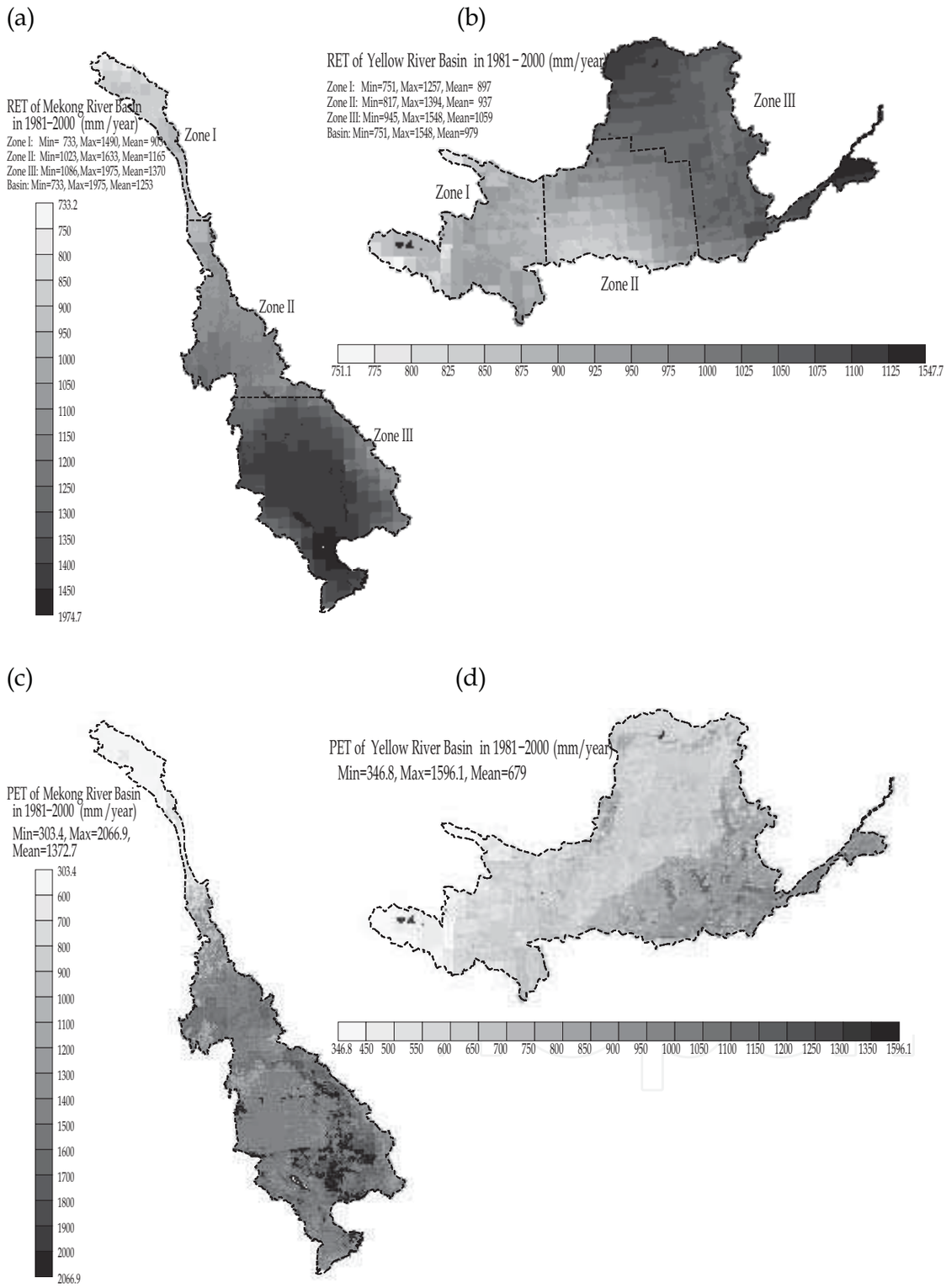

Fig. 6. Spatial distribution of annual RET and PET averaged in 1981-2000: (a) RET in Mekong; (b) RET in Yellow; (c) PET in Mekong; (d) PET in Yellow.

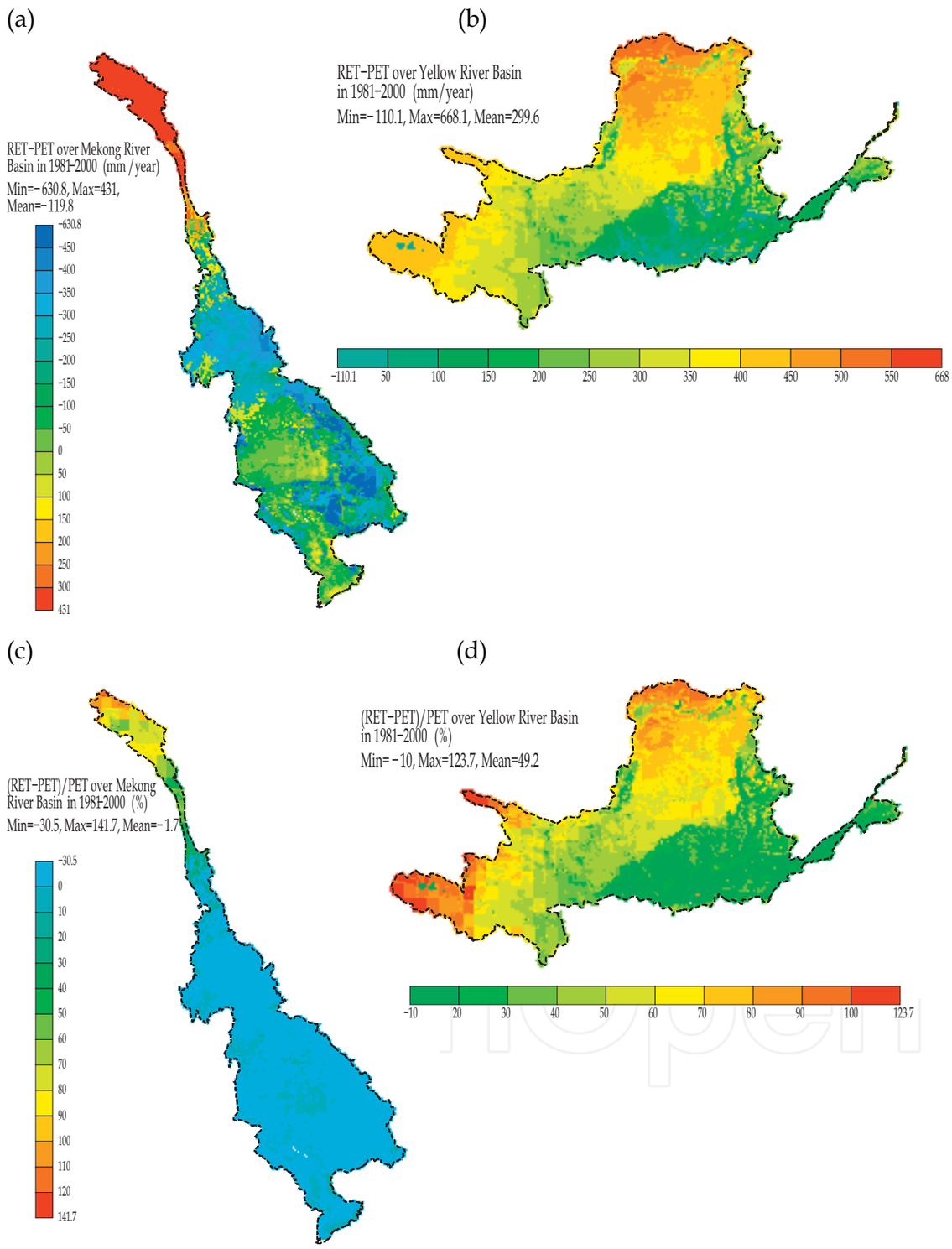

Fig. 7. Spatial distribution of the difference between annual RET and PET averaged in 1981-2000: (a) RET-PET in Mekong; (b) RET-PET in Yellow; (c) (RET-PET)/ PET in Mekong; (d) (RET-PET)/ PET in Yellow.

large amplitude because the points are located in the south of the Plateau (more precipitation). Comparing LAI_{wet} of the Loess Plateau in Figure 9(c) with the precipitation in Figures from 9(d) to 9(f), the vegetation LAI is not much related to the precipitation in the same period (P_{wet}) but well related to the antecedent precipitation in cold and dry season (P_{dry}). The cold and dry season refers to October in previous year to April the following year while the warm and wet season is from May to September. The regression R^2 is 0.5157 for LAI_{wet} vs. P_{dry} (Figure 9(a)) but 0.0228 for LAI_{wet} vs. P_{wet} (Figure 9(b)). Comparing Figure 9(c) with Figure 9(d), LAI_{wet} and P_{dry} have similar change trends, but LAI_{wet} and P_{wet} (or $P_{wet}+P_{dry}$) do not have this close relationship (Figure 9(c) vs. Figure 9(e), or Figure 9(c) vs. Figure 9(f)). This kind relationship can only be explained that: due to small potential evapotranspiration in the dry and cold season, in the form of light rainfall or snowfall, most of precipitation infiltrates to increase soil water in favor of root growing, seed germination and new bud development in spring; whereas in the warm and rainy season, because the rainfall intensity is usually heavy and the loess soil is often crusted, most of the precipitation loads flushes into the rivers and the little infiltration is consumed quickly by the strongly potential evapotranspiration. Table 3 shows that: when the years were separated into two periods, 1980's and 1990's, in average their LAI_{wet} has no difference because their P_{dry} is almost the same although their P_{wet} is different. Now we see these specific years with dry winter or wet winter. Figures 9(c) and 9(d) and Table 3 show that: in the years of 1982, 1985, 1999 and 2000, a dry antecedent winter experienced with P_{dry} less than 80 mm, their LAI_{wet} is at a very low level; whereas in the years of 1984, 1990, 1994 and 1998, a wet antecedent winter experienced with P_{dry} larger than 110 mm, their LAI_{wet} is at a high level. Precipitation in winter (P_{dry}) primarily controls vegetation condition in summer. Precipitation in summer (P_{wet}) is a secondary controlling factor, e.g. in 1985 LAI_{wet} being a bit higher due to high P_{wet} even though low P_{dry} in this dry-winter year, and in 1994 LAI_{wet} being a bit lower due to low P_{wet} even though high P_{dry} in this wet-winter year. Under a given forcing meteorological setting, high LAI means high PET. Over the middle Yellow River basin, only in summer vegetation LAI is at a bit high level. In winter, it is at a very low level.

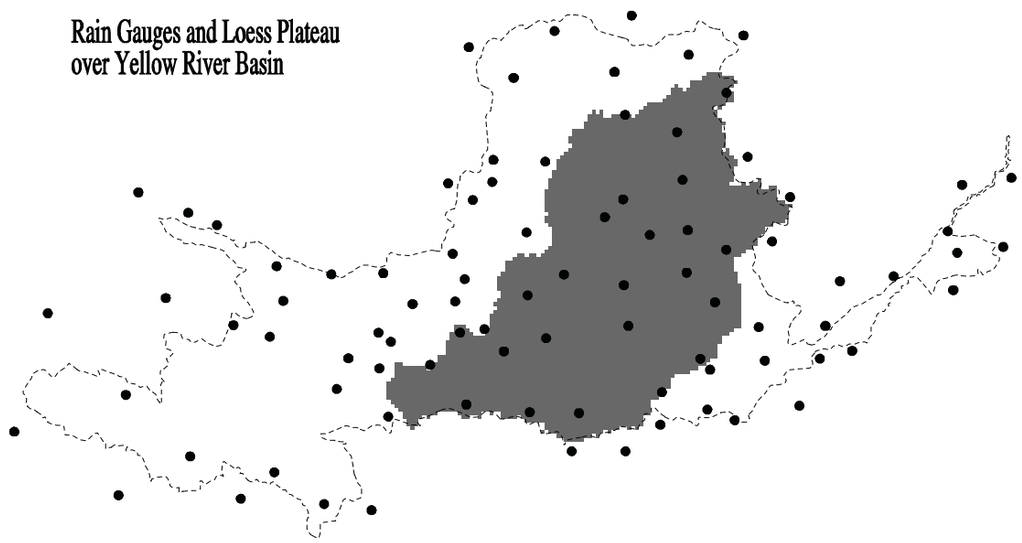

Fig. 8. Loess Plateau in the middle reaches of Yellow River (gray shaded) and rain gauges (black points)

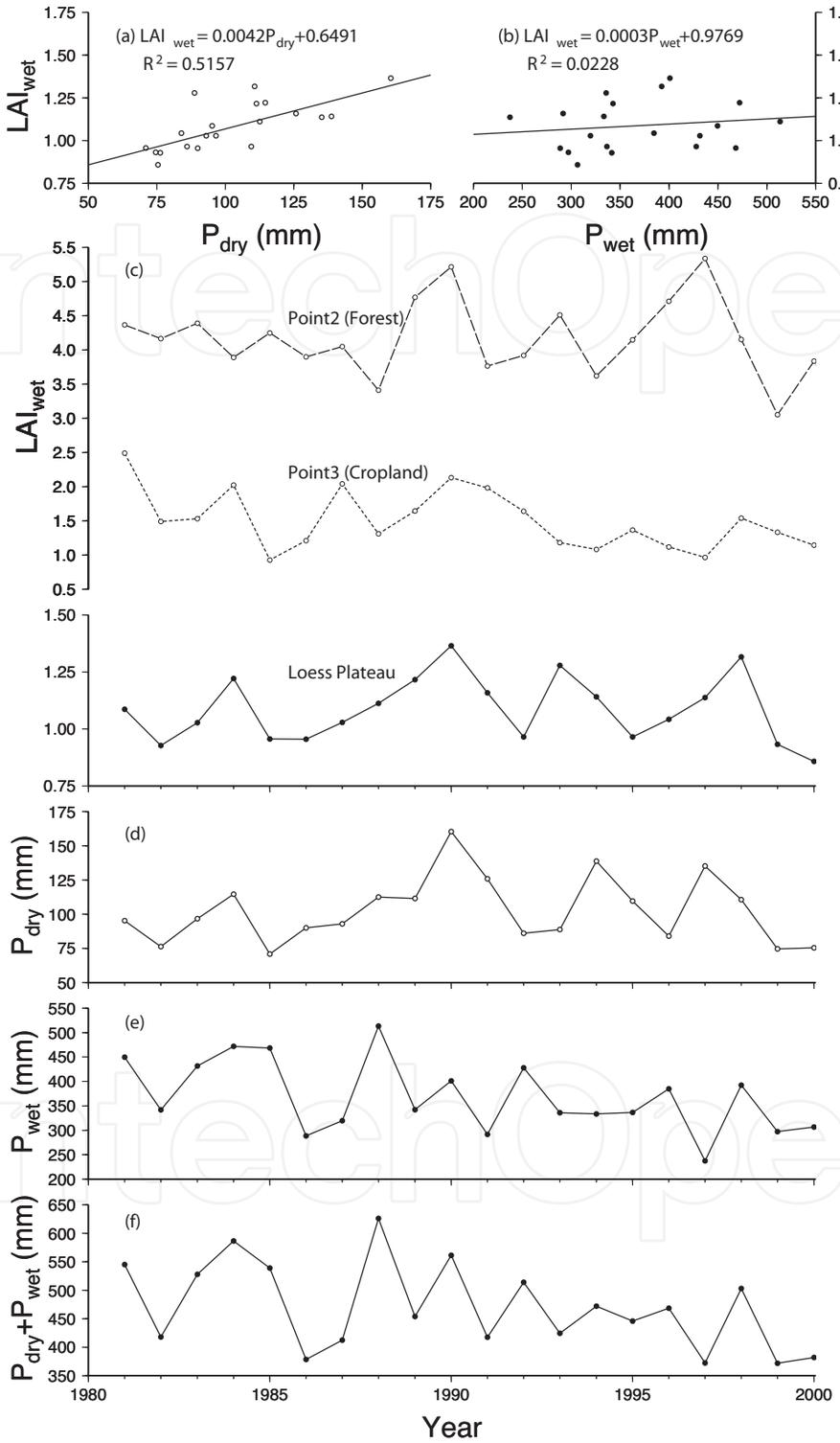

Fig. 9. Vegetation LAI_{wet} and precipitation during 1981-2000 over Loess Plateau: (a) regression relationship between LAI_{wet} and P_{dry}; (b) regression relationship between LAI_{wet} and P_{wet}; (c) LAI_{wet}; (d) P_{dry}; (e) P_{wet}; (f) $P_{dry}+P_{wet}$.

Year	LAI_{wet}	P_{dry} (mm)	P_{wet} (mm)
1981-1990	1.09	102.1	402.8
1991-2000	1.08	102.9	334.3
1982 (dry winter)	0.928	76.2	341.6
1985 (dry winter)	0.956	70.9	468.3
1999 (dry winter)	0.932	74.6	297.2
2000 (dry winter)	0.858	75.4	306.6
1984 (wet winter)	1.221	114.6	472.0
1990 (wet winter)	1.365	160.4	401.0
1994 (wet winter)	1.141	138.7	333.3
1998 (wet winter)	1.316	110.7	392.5

Table 3. Seasonal vegetation LAI and precipitation over Loess Plateau

5.4 Comparison between PET, RET and pan evaporation over Mekong River basin

The pan evaporation, E_{pan}, is available at 80 observation sites (8 in Laos, 58 in Thailand, 9 in Cambodia and 5 in Vietnam) from the Lower Mekong Hydrologic Yearbook (Interim Committee for Investigations of the Lower Mekong Basin, from 1964 to 1988). The pan type is Class A.

Figure 10 shows the comparison between annual PET, RET and E_{pan} where average monthly NDVI in period from 1981 to 2001 are used for estimates of PET and RET before 1981. As expectation, for both PET and RET, the points deviate from the 1:1 line when compared with E_{pan} (Figures 10(a) and 10(b)). Particularly for PET, the points are more scattered in total but also more aggregated with the vegetation types. This is because that the S-W method, different from the FAO-56, not only uses the climatic data but also considers the vegetation types. The less but some aggregation of the points with the vegetation type in Figure 10(b) is the result of their close location. For example, most of the forest and savannas points are located between 17.5°-20.5°N and therefore more aggregated in Figure 10(b) than the crop points which are located in a much large area. The 1:1 line seems go through the center of water surface points in Figures 10(a) and 10(b) but not representative with only one observation site (Sakon Nakhon in Thailand). The scatter is primary, especially along E_{pan} axis, and aggregation is secondary in Figures 10(a) and 10(b). It is difficult to fit a relationship between PET and E_{pan} or between RET and E_{pan} because PET or RET is an area estimate while E_{pan} is a point observation which is seriously affected by local micro-climate (e.g. often over a patch of lawn), the pan installation, its operation and maintenance. Even though these, at the crop points, PET and RET are estimated about 0.806 and 0.771 of E_{pan} respectively in average, larger than 0.7 reported by Beven (2001).

In contrast with E_{pan}, PET and RET have a good relationship, as show in Figure 10(c). The PET is larger at both forest and crop points but smaller at the savannas than RET, mainly due to the difference of their albedo (Table 1), apart due to their canopy structure (e.g. the vegetation heights and LAI). Over water surface, the points are parallel to the 1:1 line. The

very small difference is resulted from the use of different equations to convert the wind speed to 2 m height.

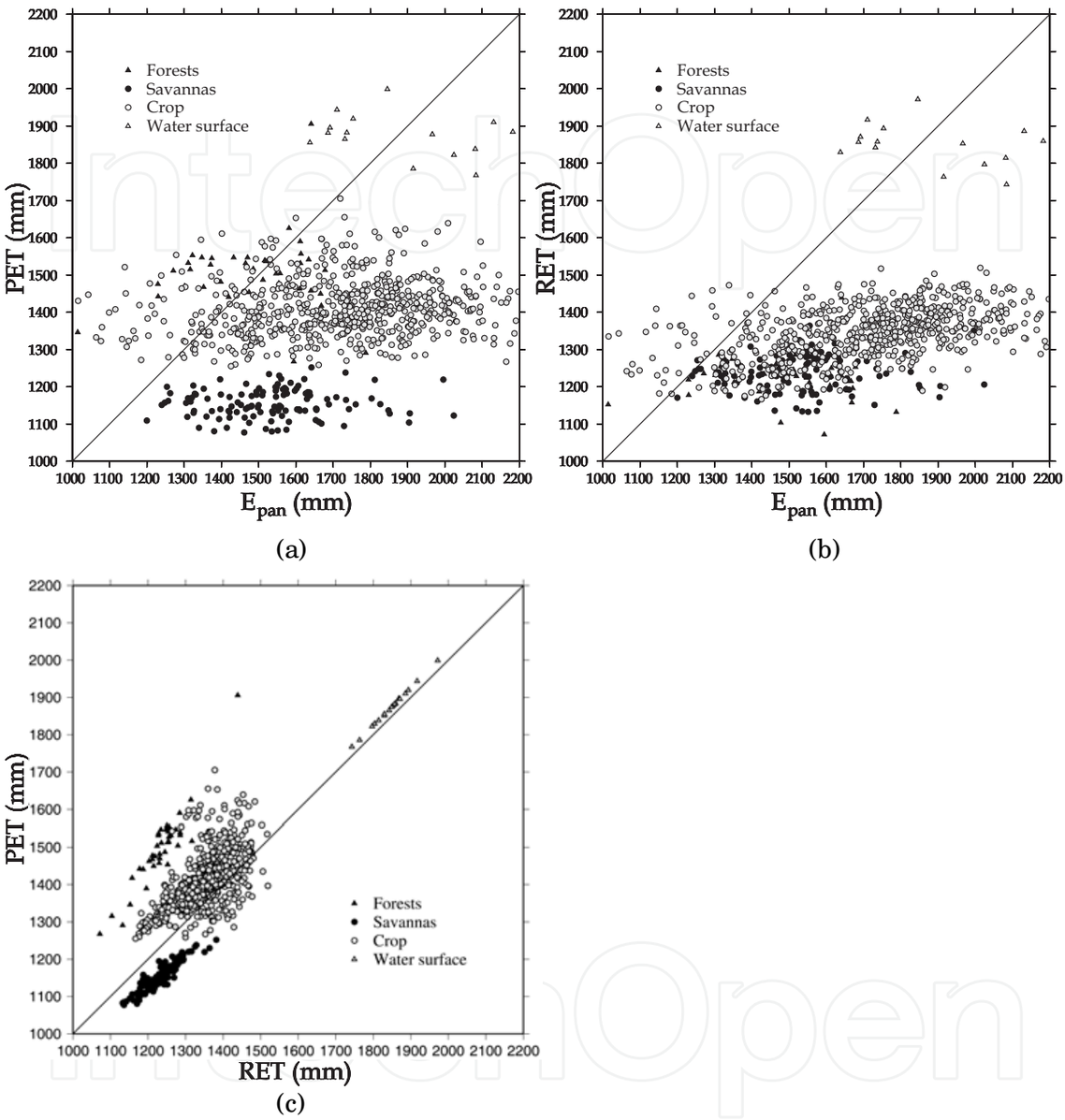

Fig. 10. Comparison among PET, RET and E_{pan} over Mekong River basin: (a) PET vs. E_{pan}, (b) RET vs. E_{pan}, and (c) PET vs. RET

5.5 Empirical relationship between FAO-56 P-M and S-W

The facts that use of the FAO-56 method is simple, and that there is a linearity between annual RET and PET over the basins and at the selected points encourage exploration for a similar relationship between monthly RET and PET using a more robust statistical analysis. In addition to the vegetation type, the LAI is the only factor used in the S-W model but not used in the FAO-56 method. Therefore, a multiple regression analysis of SPSS software was

made by categorizing the vegetation types. Because the power function was found to have good R^2 for all land covers and it satisfies PET = 0 when RET = 0, the dependent variable was used as ln(PET) and independent variables were used as IGBP land cover, ln(RET), LAI and CRU climatic variables. In order to reduce data amount and not lose their statistical attributes, not all cell data of these variables were used but randomly sampled for regression analysis over the individual basins. Of all climatic variables, only use of month precipitation and daily mean temperature in the Mekong River basin, and only use of daily mean

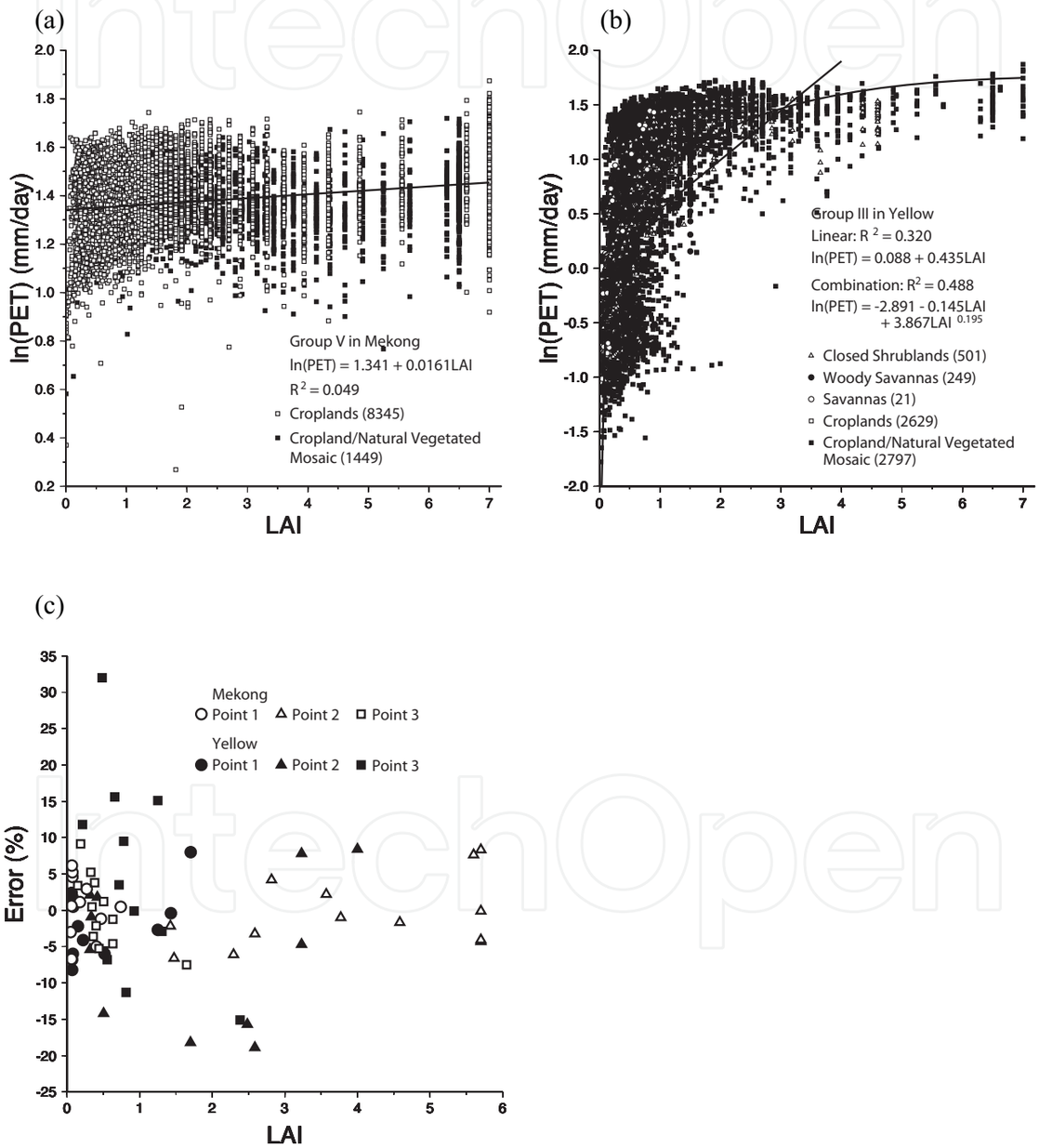

Fig. 11. Scatter plot between logarithmic PET and LAI (a) for vegetation Group V in Mekong; (b) for vegetation Group III in Yellow; and (c) prediction errors of multiple regression on three selected points corresponding to LAI.

temperature in the Yellow River basin improved the value of R^2 for some vegetation groups in the regression noticeably. Other variables gave only marginal improvement. A linear relationship seems able to describe the trend between LAI and ln(PET) in the Mekong River basin, e.g. in the case of vegetation Group V as shown in Figure 11(a). In the Yellow River basin, this relationship seems to be a combination of linear and power functions of LAI, e.g. in the case of vegetation Group III as shown in Figure 11(b). The numbers in the legend brackets in Figure 11 are the data amount sampled in the individual basins during 1981-2000 (also see "Samples" column for the same vegetation groups in Table 4). Therefore, the regression was made by further incorporating LAI in the Mekong and a combination of LAI and LAI^c in the Yellow, where c was determined by applying the SPSS "Nonlinear Regression" procedure with a function of $\ln(PET) = a + b \times LAI^c$ for each group. The multiple regression results were listed in Table 4. For the three points considered in the individual basins, the prediction errors, equal to {(PET predicted from the regression relationship between PET vs. RET and/ or other variables) – (PET estimated using the S-W model)}/ (PET estimated using the S-W model), were shown in Figure 11(c) for January to December in randomly selected years between 1981 and 2000 when NDVI data are available, to avoid the figure become a mess with too many data. Generally, by incorporating LAI, the quality of the prediction is improved to some extent, but quite large errors persist which are unrelated to LAI. We are therefore forced to the conclusion that no accurate statistical relationship exists between PET and RET because we were unable to fit a good function to account for the strongly nonlinear relationship between PET and LAI.

Category	Land cover (IGBP code)	Samples	ln(PET) = b0 + b1 × ln(RET) + b2 × Var + b3 × LAI						
			Var	b0	b1	b2	b3	R^2	σ
Group I	Evergreen Needleleaf Forest (2)	4811	P	0.03504	1.115	-3.185 E-04	0.02318	0.855	0.089
	Deciduous Broafleaf Forest (4)	1359							
	Mixed Forest (5)	3077							
Group II	Closed Shrublands (6)	536	T	-0.363	0.759	0.02186	0.06151	0.852	0.127
Group III	Woody Savannas (8)	613	No	-0.0416	0.879		0.125	0.921	0.042
Group IV	Open Shrublands (7)	123	T	-0.328	0.658	0.03964	0.123	0.989	0.061
	Grasslands (10)	2456							
	Barren or Sparsely Vegetated (16)	2							
Group V	Croplands (12)	8345	No	0.233	0.811		0.0351	0.782	0.063
	Cropland/Natural Vegetation Mosaic (14)	1449							
Group VI	Water Bodies (17)	229	No	0.002	1.007			0.999	0.002

P: monthly precipitation (mm month^{-1}); T: daily mean temperature (^{o}C); No: no climate variable significantly involved, i.e. not to improve R^2 obviously; σ: standard error (mm day^{-1}).

(a) Mekong River basin

Category	Land cover (IGBP code)	Samples	$\ln(PET) = b0 + b1 \times \ln(RET) + b2 \times T + b3 \times LAI + b4 \times LAI^c$							
			b0	b1	b2	b3	b4	c	R^2	σ
Group I	Deciduous Needleleaf Forest (2)	2	-0.955	0.802	0.0453	0.0230	-0.457	0.220	0.977	0.136
	Deciduous Broafleaf Forest (4)	462								
Group II	Mixed Forest (5)	182	-0.634	0.907	0.0397	0.0328	-0.187	0.379	0.976	0.130
Group III	Closed Shrublands (6)	501	-1.142	0.753	0.0368	0.0087	-0.668	0.195	0.979	0.120
	Woody Savannas (8)	249								
	Savannas (9)	21								
	Croplands (12)	2629								
	Cropland/Natural Vegetation Mosaic (14)	2797								
Group IV	Open Shrublands (7)	4229	-0.908	0.820	0.0232	0.192	-0.473	0.152	0.980	0.107
	Grasslands (10)	11735								
	Barren or Sparsely Vegetated (16)	110								
	Urban and Built-up (13)	7								
Group V	Water Bodies (17)	76	0.048	0.986					1.000	0.006

(b) Yellow River basin

Table 4. Multiple regression between PET (mm day^{-1}), RET (mm day^{-1}), climatic variables and LAI

5.6 Limited validation of S-W estimates with available field data

In the O Thom I watershed (area 137 km^2, elevation from 46 to 273 m, located at 105°28′E, 12°44′N) of Mekong River basin in Kompong Thom province of central Cambodia, Nobuhiro et al. (2008) measured the evapotranspiration during two distinct sampling periods in 2003 and 2004. The vegetation type is a relatively undisturbed evergreen broadleaf forest (mean tree height in the upper crown layer 27.2 m, maximum tree height 45.1 m). For the field measurement, they established a 60 m high meteorological observation tower. By using the heat balance method (incorporating the Bowen ratio) (Httori, 1985), the daily evapotranspiration levels were estimated to be 4.3 (minimum 3.0 and maximum 5.5) mm day^{-1} during 20-28 October 2003 (late rainy season), and 4.6 (minimum 2.0 and maximum 5.7) mm day^{-1} during 1-9 March 2004 (middle dry season). Arguably, the average of the two values is used as a level indicator of annual evapotranspiration, equal to 4.45 mm day^{-1}. During the observation, the water table measured shallow at a depth less than 1 m. The soil moisture was very wet. These values of measured evapotranspiration can be thought to represent the potential one. At the same site, IGBP land cover is also evergreen broadleaf forest, both in original 1-km resolution version and in the aggregated 8-km resolution version. Because field observation items by Nobuhiro et al. (2008) were not enough to apply the FAO-56 method and the S-W model, here RET and PET estimated using the data described in the section of "DATA SOURCES" are compared, averaged in the period 1981-2000. During this period, average PET was estimated to be 7.2 (from 6.3 to 7.9)

mm day^{-1} in March, 4.3 (from 3.7 to 5.1) mm day^{-1} in October, and 5.3 (from 5.1 to 5.6) mm day^{-1} for the whole year. Average RET was estimated to be 5.0 (from 4.5 to 5.4) in March, 3.4 (from 3.1 to 3.8) mm day^{-1} in October, and 3.94 (from 3.78 to 4.12) mm day^{-1} for the whole year. Obviously, comparing to the estimates of RET, which are a lot lower than the field measurement of the evapotranspiration due to the grass hypothetical crop in FAO-56 method, the estimates of PET are closer to the field measurement. The Yellow River basin is located in a semi-arid region. It is difficult to find a watershed where the LAI of vegetation cover is at a high level and soil moisture approaches field capacity for a period long enough to carry out an experiment for potential evapotranspiration measurement. Even though there is a heavy rainfall (high intensity in a short time), which happens in summer (see Figures 9(d) and 9(e), Table 3), most of it flushes into the rivers as a surface flow and the very little infiltration (due to the crusted soil surface) would be exhausted quickly by the high potential evapotranspiration. However, at the crop point (Point 3), the largest annual PET estimated from the S-W model corresponds to the most severe drought year in the last century (OSFCDRH and NWRHI, 1997).

Another way to validate the estimate of PET is applying the water balance equation to a wet basin, i.e. $\overline{ET} = \overline{P} - \overline{Q}$, where $\overline{P}$ is the precipitation, $\overline{Q}$ is the stream flow, $\overline{ET}$ is the actual evapotransipiration, all basin-averaged annual values (Donohue et al., 2007). When the basin is wetted constantly and spatially, the environment is energy-limited and $\overline{ET}$ can be a represent of PET. However, our database is not enough to support this analysis.

6. Conclusions

This chapter provides realistic estimates of potential evapotranspiration as inputs to drive hydrological modeling of large river basins, in particular for the poorly monitored or ungauged regions. For this, two extensions of P-M equation, FAO-56 method and S-W model are comparatively investigated over the Mekong and Yellow River basins, representing the humid and semi-arid Asian monsoon regions.

a. Although both are extensions of P-M equation, they use different assumptions, parameterization, and data sources to simulate different evaporation mechanisms. The estimates of RET and PET over the Mekong and Yellow River basins are spatially very different. The estimate of FAO-56 P-M is a good integrated climatic index which is able to reflect the temporal changes and spatial distribution of climate across the basins, and S-W estimate reflects the climate variability and the vegetation distribution and development.
b. Preliminary investigation into the relationship between FAO-56 P-M and S-W estimates suggest that investigating an empirical relationship between them may be worthwhile. Several attempts were made to do this, but ultimately doing so proved illusive. Large predictive errors exist because of the strong nonlinearity and scatter between PET and the LAI of the vegetation.
c. Available relevant field data are very scarce, and the only available data suggests the S-W estimate may be more realistic.

Consequently, use of the S-W model, albeit more complex, is recommended because of its more robust physical basis and because it successfully accounts for the effect of changing land surface conditions on PET. The estimated PET derived in this manner can be used to

provide a direct input to hydrological models without the need to use empirical pan or crop coefficients, which would be required if pan evaporation or RET were used.
Another finding is that: vegetation condition in summer is primarily controlled by the regional antecedent precipitation in the preceeding cold and dry seasons over the Loess Plateau in the middle reaches of the Yellow River.

Appendix A. Solar radiation

The extraterrestrial radiation is estimated from the solar constant and declination, which are the functions of the location latitude and the date in the year, expressed as follows (Shuttleworth, 1993; Allen et al., 1998).

Inverse relative distance Earth-Sun:

$$d_r = 1 + 0.033\cos\left(\frac{2\pi}{365}J\right) \tag{A1}$$

where J is Julian day in the year, corresponding to the middle day of the interval.

Solar declination:

$$\delta = 0.409\sin\left(\frac{2\pi}{365}J - 1.39\right) \text{ in rad} \tag{A2}$$

Sunset hour angle:

$$\omega_s = \arccos\left[-\tan(\varphi)\tan(\delta)\right] \text{ in rad} \tag{A3}$$

where φ is the location latitude in radians.

Extraterrestrial radiation in a day:

$$R_a = \frac{24(60)}{\pi} G_{sc} d_r \left[\omega_s \sin(\varphi)\sin(\delta) + \cos(\varphi)\cos(\delta)\sin(\omega_s)\right] \tag{A4}$$

where R_a is in MJm^{-2} day^{-1} and G_{sc} is the solar constant, G_{sc} = 0.082 MJm^{-2} min^{-1}.

Solar radiation over vegetation canopy:

$$R_{solar} = \left(a_s + b_s \frac{n}{N}\right) R_a \tag{A5}$$

where n/N is calculated using Equation (50), the parameters a_s and b_s are set to 0.25 and 0.50 respectively when their measurements are lack.
The clear-sky solar radiation is calculated as:

$$R_{solar}^{0} = \left(0.75 + 2 \times 10^{-5} z\right) R_a \tag{A6}$$

where z is the elevation above sea level (m)

7. Acknowledgements

We are pleased to acknowledge the financial support of the President Scientific Funds of South China Agricultural University through the research project 'Development of a distributed watershed hydrological model and integrated management of water resources' (7600-K07050), and of the Department of Education of Guangdong Province through the research project 'Non-point source pollution of Hanjiang River basin and the distributed hydrological and environmental simulation' (2008-86), and of the Scientific Innovation Funds of Department of Water Resources of Guangdong Province through the research project 'Application research of distributed hydrological model and data assimilation in Hanjiang River water resources and water quality' (2009).

8. References

Allen, R. G., Pereira, L. S., Raes, D. and Smith, M. (1998) Crop evapotranspiration — guidelines for computing crop water requirements. FAO Irrigation and Drainage Paper, No. 56, FAO, Rome.

Allen, R. G., Smith, M., Perrier, A. and Pereira, L. S. (1993) Updated reference evapotranspiration definition and calculation procedures, Revision of FAO Methodologies for Crop Water Requirements. 36 pp.

Allen, S. J. (1994) An update for calculation of the reference evapotranspiration. ICID Bull., 43(2), 35-91.

Andersen, J., Dybkjaer, G., Jensen, K. H., Refsgaard, J. C. and Rasmussen, K. (2002) Use of remotely sensed precipitation and leaf area index in a distributed hydrological model. J. Hydrol., 264, 34-50.

Beven, K. J. (2001) Rainfall-Runoff Modelling, the Primer. John Wiley, Chichester (England), 360 pp.

Braud, I., Dantas-Antonino, A. C., Vauclin, M., Thony, J. L. and Ruelle, P. (1995) A simple soil-plant-atmosphere transfer model (SiSPAT) development and field verification. J. Hydrol., 166, 213-250.

Brisson, N., Itier, B., L'Hotel, J. C. and Lorendeau, J. Y. (1998) Parameterisation of the Shuttleworth-Wallace model to estimate daily maximum transpiration for use in crop models. Ecol. Model., 107, 159-169.

Brutsaert, W. (1982) Evaporation into the Atmosphere. D. Reidel, Dordrecht, Holland, 299 pp.

Calder, I. R., Narayanswamy, M. N., Sirinivasalu, N. V., Darling, W. G. and Lardner, A. J. (1986) Investigation into the use of deuterium as a tracer for measuring transpiration from eucalyptus. J. Hydol., 84, 345-351.

Camillo, P. J. and Gurney, R. J. (1986) A resistance parameter for bare soil evaporation models. Soil Sci., 141, 95-106.

Choudhury, B. J. and Monteith, J. L. (1988) A four-layer model for the heat budget of homogeneous land surfaces. Quart. J. Royal Meteorol. Soc., 114, 373-398.

Danko, D. M. (1992) The digital chart of the world. GeoInfo Systems 2, 29-36.

De Ridder, K. and Schayes, G. (1997) Radiative transfer in the IAGL land surface model. J. Appl. Meteorol., 36, 12-21.

Denmead, O. T. (1976) Temperate cereals. In: J. L. Monteith (Editor), Vegetation and the Atmosphere, Vol. 2. Academic Press, 31 pp.

Dickinson, R. E. (1984) Modeling evapotranspiration for three-dimensional global climate models. In: J. E. Hanson, T. Takahashi (Editor), Climate Processes and Climate Sensitivity. Amer. Geophys. Union, 58-72.

Donohue, R. J., Roderick, M-. L. and McVicar, T. R. (2007) On the importance of including vegetation dynamics in Budyko's hydrological model. Hydrol. Earth System Sci. 11, 983-995.

Doorenbos, J. and Pruitt, W. O. (1992) Crop water requirements. FAO Irrigation and Drainage. Paper, No. 24, FAO, Rome, 144 pp.

Dunn, S. M. and Mackay, R. (1995) Spatial variation in evapotranspiration and the influence of land use on catchment hydrology. J. Hydrol., 171, 49-73.

Farahani, H. J. and Bausch, W. C. (1995) Performance of evapotranspiration models for maize – bare soil to closed canopy. Trans. ASAE, 38, 1049-1059.

Federer, C. A., Vorosmarty, C. J. and Fekete, B. (1996) Intercomparison of methods for potential evapotranspiration in regional or global water balance models. Water Resour. Res., 32, 2315-2321.

Fennessey, N. M. and Kirshen, P. H. (1994) Evaporation and evapotranspiration under climate change in New England. J. Water Resour. Plann. Manage., 120(1), 48-69.

Fuchs, M. and Tanner, C. B. (1968) Evaporation from a drying soil. J. Appl. Meteorol., 6, 852-857.

Gardiol, J. M., Serio, L. A. and Maggiora, A. I. D. (2003) Modeling evapotranspiration of corn (Zea mays) under different plant densities. J. Hydrol., 217, 188-196.

Granger, R. J. (1989) An examination of the concept of potential evaporation. J. Hydrol. 111, 9-19.

Hattori, S. (1985) Explanation on derivation process of equations to estimate evapotranspiration and problems on the application to forest stand. Bull. Forestry and Forest Products Research Institute 332, 139-165 (in Japanese).

Hess, T. M. (1998) Trends in reference evapotranspiration in the North East Arid Zone of Nigeria, 1961-91. J. Arid Envir., 38, 99-115.

Hiller, D. (1980) Applications of Soil Physics. Academic, San Diego, Clifo., 385 pp.

Huntingford, C. (1995) Non-dimensionalisation of the Penman-Monteith model. J. Hydrol., 170, 215-232.

Hutchinson, M. F. (1995) Interpolating mean rainfall using thin plate smoothing splines. Int. J. Geogr. Inform. Systems, 9, 385–403.

Interim Committee for Investigations of the Lower Mekong Basin, from 1964 to 1988.

Iritz, Z., Lindroth, A., Heikinheimo, M., Grelle, A. and Kellner, E. (1999) Test of a modified Shuttleworth-Wallace estimate of boreal forest evaporation. Agri. Forest Meteorol., 98-99, 605-619.

Jarvis, P. G. (1976) The interpretation of the variation in leaf water potential and stomatal conductance found in canopies in the field. Phil. Trans. Royal Soc. London, B 273, 593-610.

Jones, H. G. (1992) Plants and microclimate: a quantitative approach to environmental plant physiology, 2nd ed. Cambridge University Press, New York, 428 pp.

Kelliher, F. M., Leuning, R., Raupach, M. R. and Schulze, E. –D. (1995) Maximum conductances for evaporation from global vegetation types. Agri. Forest Meteorol., 73, 1-16.

Kite, G. (2001) Modeling the Mekong: hydrological simulation for environmental impact studies. J. Hydrol., 253, 1-13.

Kondo, J., Saigusa, N. and Sato, T. (1990) A parameterization of evaporation from bare soil surface. J. Appl. Meteorol., 29, 383-387.

Korner, G., Schell, J. A. and Bauer, H. (1979) Maximum leaf diffusive conductance in vascular plants. Photosynthesis, 13(1), 45-82.

Lafleur, P. M. and Rouse, W. R. (1990) Application of an energy combination model for evaporation from sparse canopies. Agri. Forest Meteorol., 49, 135-153.

Lhomme, J. -P. (1997) Towards a rational definition of potential evaporation. Hydrol. Earth System Sci., 1, 257-264.

Lhomme, J. –P., Elguero, Chehbouni, A. and Boulet, G. (1998) Stomatal control of transpiration: Examination of Monteith's formulation of canopy resistance. Water Resour. Res., 34(9), 2301-2308.

Liang, X., Lettenmaier, D. P., Wood, E. F. and Burges, S. J. (1994) A simple hydrologically based model of land surface water and energy fluxes for general circulation models. J. Geophy. Res., 99(D7), 14415-14428.

Loveland, T. R., Reed, B. C., Brown, J. F., Ohlen, D. O., Zhu, J., Yang, L., and Merchant, J. W. (2000) Development of a Global Land Cover Characteristics Database and IGBP DISCover from 1-km AVHRR Data. Int. J. Remote Sensing, 21, 1303-1330.

Lund, M. R. and Soegaard, H. (2003) Modelling of evaporation in a sparse millet crop using a two-source model including sensible heat advection within the canopy. J. Hydrol., 280, 124-144.

Mahfouf, J. F. and Noilhan, J. (1991) Comparative study of various formulations of evaporation from bare soil using in situ data. J. Clim. Appl. Meteorol., 30(9), 1354-1365.

Mauser, W. and Schadlich, S. (1998) Modelling the spatial distribution of evapotranspiration on different scales using remote sensing data. J. Hydrol., 212-213, 250-267.

McNaughton, K. G. and Black, T. A. (1973) A study of evapotranspiration from a Douglas Fir forest using the energy balance approach. Water Resour. Res., 9, 1579-1590.

McVicar, T. R., Van Niel, T. G., Li, L. T., Hutchinson, M. F., Mu, X. M. and Liu, Z. H. (2007) Spatially Distributing Monthly Reference Evapotranspiration and Pan Evaporation Considering Topographic Influences. J. Hydrol., 338, 196-220.

McVicar, T. R., Van Niel, T. G., Li, L. T., Roderick, M. L., Rayner, D. P., Ricciardulli, L. and Donohue, R. J. (2008) Wind speed climatology and trends for Australia, 1975-2006: Capturing the stilling phenomenon and comparison with near-surface reanalysis output. Geophy. Res. Letters, 35, L20403.

Mo, X., Liu, S., Lin, Z. and Zhao, W. (2004) Simulating temporal and spatial variation of evapotranspiration over the Lushi basin. J. Hydrol., 285, 125-142.

Monteith, J. L. (1965) Evaporation and environment. Symp. Soc. Exp. Bio. XIX, 205-234, Cambridge University Press.

Monteith, J. L. (1973) Principles of environmental physics. Edward Arnold, London, 214 pp.

Monteith, J. L. (1981) Evaporation and surface temperature. Quart. J. Royal Meteorol. Soc., 107, 1-27.

Monteith, J. L. (1995) Accommodation between transpiring vegetation and the convective boundary layer. J. Hydrol., 166(3-4), 251-263.

Myneni, R. B. and Williams, D. L. (1994) On the relationship between FPAR and NDVI. Remote Sensing Environ., 49, 200-211.

New, M., Hulme, M. and Jones, P. (1999) Representing twentieth-century space-time climate variability. Part I: Development of a 1961-90 mean monthly terrestrial climatology. J. Climate, 12, 829-856.

New, M., Hulme, M. and Jones, P. (2000) Representing twentieth-century space-time climate variability. Part II: Development of 1901-96 monthly grids of terrestrial surface climate. J. Climate, 13, 2217-2238.

Nobuhiro, T., Shimizu, A., Kabeya, N., Tamai, K., Ito, E., Araki, M., Kubota, T., Tsuboyama, Y. and Chann, S. (2008) Evapotranspiration during the late rainy season and middle of the dry season in the watershed of an evergreen forest area, central Cambodia. Hydrol. Process., 22(9), 1281-1289.

Noilhan, J. and Planton, S. (1989) A simple parameterization of land surface process for meteorological models. Mon. Weather Rev., 17, 536-549.

OSFCDRH (Office of State Flood Control and Drought Relief Headquarters) and NWRHI (Nanjing Water Resources & Hydrology Institute) (1997) China's Flood and Drought Disaster. Water Resources and Hydropower Press, Bejing (in Chinese).

Penman, H. L. (1948) Natural evaporation from open water, bare soil and grass. Proc. Royal Soc. London, A 193, 120-146.

Priestley, C. H. B. and Taylor, R. J. (1972) On the assessment of surface heat flux and evaporation using large-scale parameters. Monthly Weather Review, 100, 81-92.

Raupach, M. R. (1995) Vegetaion-atmosphere interaction and surface conductance at leaf, canopy and regional scales. Agri. Forest Meteorol., 73, 151-179.

Rawls, W. J. and Brakensiek, D. L. (1985) Prediction of soil water properties for hydrologic modeling. Watershed Management in the Eighties, ASCE, pp. 293-299.

Ross, J. (1975) Radiative transfer in plant communities. In: J. L. Monteith (Editor), Vegetation and the Atmosphere. Academic Press, London, pp. 13-55.

Rowntree, P. R. (1991) Atmospheric parameterization schemes for evaporation over land: basic concepts and climate modeling aspects. In: T. J. Schmugge, J. -C. Andre (Editors), Land Surface Evaporation: Measurement and Parameterization, p. 5-29.

Sellers, P. J., Los, S. O., Tucker, C. J., Iustice, C. O., Dazlich, D. A., Collatz, G. J. and Randall, D. A. (1996) A revised land surface parameterization (SiB2) for atmospheric GCMs. Part II: the generation of global fields of terrestrial biophysical parameters from satellite data. J. Climate, 9, 706-737.

Sellers, P. J., Tucker, P. J., Collatz, G. J., Los, S. O., Justice, C. O., Dazlich, D. A. and Randall, D. A. (1994) A global 1 degree by 1 degree NDVI data set for climate studies. Part 2: the generation of global fields of terrestrial biophysical parameters from NDVI. Int. J. Remote Sensing, 15(17), 3519-3545.

Shen, Y., Kondoh, A., Tang, C., Zhang, Y., Chen, J., Li, W., Sakura, Y., Liu, C., Tanaka, T. and Shimada, J. (2002) Measurement and analysis of evapotranspiration and surface conductance of a wheat canopy. Hydrol. Process., 16, 2173–2187.

Shuttleworth, W. J. (1993) Evaporation. In: D.R. Maidment (Editor), Handbook of Hydrology. McGraw-Hill, New York, pp. 4.1-4.53.

Shuttleworth, W. J. and Gurney, R. J. (1990) The theoretical relationship between foliage temperature and canopy resistance in sparse crops. Quart. J. Royal Meteorol. Soc., 116, 497-519.

Shuttleworth, W. J. and Wallace, J. S. (1985) Evaporation from sparse crops - an energy combination theory. Quart. J. Royal Meteorol. Soc., 111, 839-855.

Stannard, D. I. (1993) Comparison of Penman-Monteith, Shuttleworth-Wallace, and Modified Priestley-Taylor evapotranspiration models for wildland vegetation in semiarid rangeland. Water Resour Res., 29(5), 1379-1392.

Stewart, J. B. (1988) Modelling surface conductance of pine forest. Agri. Forest Meteorol., 43, 19-35.

Stewart, J. B. and Gay, L. W. (1989) Preliminary modeling of transpiration from the FIFE site in Kansas. Agri. Forest Meteorol., 48, 305-315.

Sun, S. F. (1982) Moisture and heat transport in a soil layer forced by atmospheric conditions. M. Sc. Thesis, Dept. of Civil Engineering, University of Connecticut, 72 pp.

Thornthwaite, C. W. (1948) An approach toward a rational classification of climate. Geograophical Rev., 38, 55-94.

Tourula, T. and Heikinheimo, M. (1998) Modelling evapotranspiration from a barley field over the growing season. Agri. Forest Meteorol., 91, 237-250.

Tucker, C. J., Pinzon, J. E., Brown, M. E., Slayback, D., Pak, E. W., Mahoney, R., Vermote, E. and El Saleous, N. (2005) An extended AVHRR 8-km NDVI data set compatible with MODIS and SPOT vegetation NDVI data. Int. J. Remote Sensing, 26(20), 4485-5598.

Uchijima, Z. (1976) Maize and Rice. In: J. L. Monteith (Editor), Vegetation and the Atmosphere, Vol. 2. Academic Press, New York, pp. 33-64.

van de Griend, A. A. and Owe, M. (1994) Bare soil surface resistance to evaporation by vapor diffusion under semiarid conditions. Water Resour. Res., 30(2), 181-188.

Vazquez, R. F. and Feyen, J. (2003) Effect of potential evapotranspiration estimates on effective parameters and performance of the MIKE SHE-code applied to a medium-size catchment. J. Hydrol., 270, 309-327

Verdin, K. L. and Greenlee, S. K. (1996) Development of continental scale digital elevation models and extraction of hydrographic features. In: Proceedings, Third International Conference/ Workshop on Integrating GIS and Environmental Modeling, Santa Fe, New Mexico, January 21-26, 1996. National Center for Geographic Information and Analysis, Santa Barbara, California.

Verma, S. B., Baldocchi, D. D., Anderson, D. E., Matt, D. R. and Clement, R. J. (1986) Eddy fluxes of CO_2, water vapour, and sensible heat over a deciduous forest. Boundary-Layer Meteorol., 36, 71-91.

Vorosmarty, C. J., Federer, C. A. and Schloss, A. L. (1998) Potential evaporation functions compared on US watersheds: possible implications for global-scale water balance and terrestrial ecosystem modeling. J. Hydrol., 207, 147-169.

Vourlitis, G. L., Filho, N. P., Hayashi, M. M. S., Nogueira, J. S., Caseiro, F. T. and Campelo, J. H. (2002) Seasonal variations in the evapotranspiration of a transitional tropical forest of Mato Grosso, Brazil. Water Resour. Res., 38(6), 1094,

Wilson, R. and Shaw, R. (1977) A higher order closure model for canopy flow. J. Appl. Meteorol., 16, 1197-1205.

WRI, IUCN and IWMI, the Ramsar Convention Bureau, 2003. The Watersheds of the World_CD. World Resources Institute, Washington, DC. http:/ / www.waterandnature.org/ eatlas

SUGGESTED READINGS

Zhou, Maichun, Ishidaira, Hiroshi and Takeuchi, Kuniyoshi (2006) Estimating the potential evapotranspiration over the Yellow River basin by considering the land cover characteristics. IAHS RedBook No. 303 (Predictions in Ungauged Basins: Promises and Progress, edited by M. Sivapalan), p. 214-225, Proceedings of symposium S7 held during the Seventh IAHS Scientific Assembly at Foz do Iguassu, Brazil, April 2005.

Zhou, M. C., Ishidaira, H., Hapuarachchi, H. P., Magome, J., Kiem, A. S. and Takeuchi, K. (2006) Estimating potential evapotranspiration using Shuttleworth-Wallace model and NOAA-AVHRR NDVI data to feed a distributed hydrological model over the Mekong River Basin. Journal of Hydrology, 327, 151-173.

Zhou, M. C., Ishidaira, H. and Takeuchi, K. (2007) Estimation of potential evapotranspiration over Yellow River basin: reference crop evaporation or Shuttleworth-Wallace? Hydrological Processes, 21(14), 1860-1874.

Zhou, M. C., Ishidaira, H. and Takeuchi, K. (2008) Comparative study of potential evapotranspiration and interception evaporation by land cover over Mekong basin. Hydrological Processes, 22(9), 1290-1309.

Zhou, Maichun, Ishidaira, Hiroshi, Takeuchi, Kuniyoshi and Gao, Yongtong (2009) Evapotranspiration in the Mekong and Yellow River basins. Hydrological Sciences Journal, 54(3), 623-638.

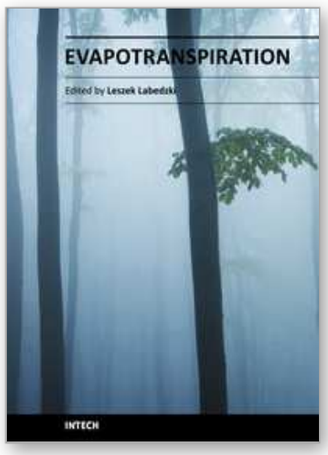

Evapotranspiration

Edited by Prof. Leszek Labedzki

ISBN 978-953-307-251-7
Hard cover, 446 pages
Publisher InTech
Published online 16, March, 2011
Published in print edition March, 2011

Evapotranspiration is a very complex phenomenon, comprising different aspects and processes (hydrological, meteorological, physiological, soil, plant and others). Farmers, agriculture advisers, extension services, hydrologists, agrometeorologists, water management specialists and many others are facing the problem of evapotranspiration. This book is dedicated to further understanding of the evapotranspiration problems, presenting a broad body of experience, by reporting different views of the authors and the results of their studies. It covers aspects from understandings and concepts of evapotranspiration, through methodology of calculating and measuring, to applications in different fields, in which evapotranspiration is an important factor. The book will be of benefit to scientists, engineers and managers involved in problems related to meteorology, climatology, hydrology, geography, agronomy and agricultural water management. We hope they will find useful material in this collection of papers.

INTECH
open science | open minds

InTech Europe
University Campus STeP Ri
Slavka Krautzeka 83/A
51000 Rijeka, Croatia
Phone: +385 (51) 770 447
Fax: +385 (51) 686 166
www.intechopen.com

InTech China
Unit 405, Office Block, Hotel Equatorial Shanghai
No.65, Yan An Road (West), Shanghai, 200040, China
中国上海市延安西路65号上海国际贵都大饭店办公楼405单元
Phone: +86-21-62489820
Fax: +86-21-62489821

IntechOpen